GEOLOGICAL SURVEY OF CANADA
OPEN FILE 6713

Focal Mechanisms and Depths of Aftershocks of the 2010 Haiti Earthquake

A. L. Bent

2011

Natural Resources Canada | Ressources naturelles Canada

Canada

GEOLOGICAL SURVEY OF CANADA
OPEN FILE 6713

Focal Mechanisms and Depths of Aftershocks of the 2010 Haiti Earthquake

A. L. Bent

2011

doi:10.4095/288018

This publication is available from the Geological Survey of Canada Bookstore (http://gsc.nrcan.gc.ca/bookstore_e.php).
It can also be downloaded free of charge from GeoPub (http://geopub.nrcan.gc.ca/).

Recommended citation
Bent, A. L., 2011. Focal Mechanisms and Depths of Aftershocks of the 2010 Haiti Earthquake; Geological Survey of Canada, Open File 6713, 32 p.

Publications in this series have not been edited; they are released as submitted by the author.

Abstract

The devastating magnitude 7.0 earthquake that struck Haiti on 12 January 2010 was followed by hundreds of aftershocks. The largest were recorded at regional to teleseismic distances. The smaller aftershocks were not recorded in the days immediately following the mainshock as there was no seismic monitoring capacity within Haiti. With the installation of a real time three-station network in Haiti by the GSC in mid-February the ability to monitor the aftershocks was vastly improved. Using the new Haitian stations as well as existing stations elsewhere in the Caribbean, focal mechanisms and depths of many of the aftershocks can be determined, both of which provide insight into the seismotectonics of the region and implications for future seismic hazard assessments. This paper summarizes the focal mechanisms and depths of the larger (magnitude ≥ 4.5) aftershocks determined by regional moment tensor inversion and the focal mechanisms of the smaller aftershocks determined by a composite first motion inversion. The results are consistent with the teleseismically determined focal mechanisms of the mainshock and largest aftershock and provide further evidence for a complex faulting regime consisting of strike-slip faulting in the east of the aftershock zone where the mainshock initiated and thrust faulting in the west where the largest number of aftershocks has occurred.

Introduction

At 2153 UT (1653 local time) on 12 January 2010 a magnitude 7.0 earthquake occurred 25 km WSW of Port-au-Prince, Haiti. The earthquake resulted in nearly a quarter of million deaths and caused widespread destruction throughout southern Haiti. Although no surface rupture was found, the earthquake was widely believed to have occurred on the Enriquillo-Plaintain Garden Fault (EPGF; Figure 1), a fault which makes up part of the boundary between the North American and Caribbean plates and which is known to have generated comparable earthquakes in the past. A more detailed summary of the earthquake may be found on the United States Geological Survey (USGS, 2010) website and a very thorough description of the EPGF in Mann et al (1995).

It had been more than one hundred years since the last major earthquake in Haiti, and due to a lack of routine seismic monitoring in that country little is known about the background seismicity making reliable hazard assessments difficult. Seismograph stations deployed in Haiti after the earthquake have been recording its numerous aftershocks, most of which are too small to be recorded at larger distances. Analyzing the aftershocks and longer term monitoring of seismic activity in Haiti should provide improved seismic hazard assessments for Haiti. In particular, reliable magnitude recurrence rates may be established and more detailed analysis of the individual aftershocks should provide additional information about the seismotectonic processes in the region of the Enriquillo-Plaintain Garden Fault system.

The relative motion between the North American and Caribbean plates along the EPGF is primarily left-lateral strike slip (Manaker et al 2008; Mann et al, 1995, 2002). The focal mechanism of the mainshock (Global CMT, 2010; USGS, 2010) is consistent with this motion. The focal mechanism of the largest, magnitude 6.0, aftershock, however, is indicative of nearly pure thrust faulting suggesting that the motion along and near the plate boundary is more complex. The thrust faulting may be occurring on a landward extension of the South Haiti Fault discussed by Mann et al (2002).

Many groups have undertaken studies of the mainshock (among them, Eberhard et al, 2010; Hjorleifsdöttir and Nettles, 2010; Lin et al, 2010; Seeber and Waldhauser, 2010). Less attention has been paid to the aftershocks. This study focuses on the aftershocks and in particular on their focal mechanisms and depths, which provide information about the fault(s) on which they occur. This report is intended as a preliminary summary of the aftershock focal mechanisms determined by regional moment tensor inversion and first motion analysis. It is anticipated that a more detailed paper will follow, which will include the results and a more in depth analysis of the focal mechanism project as well as several additional ongoing studies of Haiti by this author and several GSC colleagues, some of which have been briefly summarized by Bent et al (2010), Cassidy et al (2010) and McCormack et al (2010).

Seismograph Stations and Data

Approximately one month after the mainshock, NRCAN's Canadian Hazard Information Service (CHIS) installed three seismograph stations in Haiti. The stations (Figure 2) are located in Port-au-Prince (PAPH), Jacmel (JAKH) and Léogâne (LGNH). Each site consists of a three component broadband seismometer as well as a three component strong motion accelerometer. All instruments are continuously recording at 100 samples per second and data are transmitted in real time via satellite to Ottawa, where they are archived and

forwarded to other groups, including the USGS and the Caribbean Tsunami Warning System. Additional stations were installed by the USGS but data from most are not available in real time as is also the case for a series of ocean bottom seismometers (OBS) and four land seismometers deployed by a French research team (GéoAzur).

As is their practice for global earthquakes, the USGS routinely determines the locations and magnitudes of only those aftershocks of magnitude 4.5 or greater. Focal mechanisms tend to be determined by the USGS and the Global CMT Project only for the earthquakes of approximately magnitude 5.0 or greater although smaller earthquakes of particular interest are sometimes analyzed.

Using data from the three Haitian stations and supplementing the dataset when appropriate with data from additional Caribbean stations (GRTK, GTBY and SDDR; Figure 2), the GSC has been making an effort to locate as many of the smaller aftershocks as possible. The arrival times and magnitudes are forwarded to the International Seismological Centre (ISC) where they can be catalogued and where data from other stations may be added to improve the solutions. To date, more than 700 aftershocks have been located (National Earthquake Database, 2010; hereafter referred to as the NEDB). The solutions are also archived by the GSC and posted on the internet: http://earthquakescanada.nrcan.gc.ca/haiti/index-eng.php

This paper is focused primarily on the moderate-sized aftershocks. That is, those too small to be evaluated by research groups employing teleseismic data but for which regional data may be used to determine depths and focal mechanisms. These earthquakes are generally in the magnitude 4.5 to 5.0 range. Some attempt has also been made to analyze the smaller events albeit in somewhat less detail.

Regional Moment Tensors

For aftershocks large enough to be recorded at regional distances (150-1500 km) but too small to have good teleseismic signals, a regional moment tensor inversion may be used to determine the focal mechanism as well as the depth and moment magnitude. Moment tensor inversions were performed for thirteen aftershocks of magnitude 4.5 or greater. The USGS locations and origin times were assumed. Small errors in location will not adversely affect the solution. The largest events were not analyzed as they had been previously evaluated by one or more groups (USGS (2010), Global CMT Project (2010)) using teleseismic data. Not all magnitude 4.5+ events in the USGS database were analyzed. The first events analyzed were those that occurred after the Canadian stations had been deployed in an attempt to determine a relation between M_L and M_W. The number of events was too small for any conclusions on this topic to be robust. The project was extended to include more of the early aftershocks when it appeared that they were not being studied by other research groups. Most of the magnitude 4.5 and greater events occurring more than a few days after the mainshock have been analyzed. Not all of those occurring within the first 48 hours following the mainshock have been evaluated. Events within this time frame were selected with the intent of improving the geographic coverage of events analyzed and an attempt was made to avoid any aftershocks whose signal was likely to be buried in the coda of a larger or previous event. The events for which focal mechanisms were determined in this study are summarized in the Table.

Data from four regional stations (BCIP, GRTK, GTBY and SDDR; Figure 2) at four different

azimuths were accessed via the IRIS-DMC. The regional moment tensor code of Kao et al (1998) was used to determine the depth, focal mechanism and moment magnitude. The velocity model used for routine earthquake locations in Puerto Rico (Huerfano and Bataille, 1994) was selected as a representative regional model. It is noted that this model may not be ideal for the path to GRTK which crosses the subduction zone. The initial inversion was run using all available components and stations. If the solution provided very poor fits to the data for some components, these components were down-weighted and the inversion was rerun. It should be noted however, that these components are still considered when the overall misfit is calculated and also that excluding these components did not radically alter the initial solution (focal mechanism, depth, moment) but only the fit to the solution.

The focal mechanisms (Figures 4a-4m) determined via the regional moment tensor inversion are consistent geographically with the teleseismic solutions for the large events and with the composite solutions for the smaller ones. Again, there is evidence for thrust faulting in the west and strike-slip in the east. Most events have at least one nodal plane whose strike corresponds roughly to that of the EPGF but this fact should not be taken as proof that the events occurred on it.

The depths range from 2 km to 15 km with most in the 5-10 km range, which corresponds to the shallow to mid-crust. Most depths are constrained to within a few km although there are a few events for which the depths are not well constrained (see insets in Figures 4a-4m). There is no obvious geographic trend to the depths which could be used to infer the dip direction or angle of the fault(s) on which the earthquakes occurred. The depths and mechanisms are consistent with those determined by Seeber and Waldhauser (2010) and Waldhauer et al (2010) using a dataset consisting of earthquakes that occurred early in the aftershock sequence.

For the most part, m_b and M_W are within 0.2 magnitude units of each other (Table). There are a few events for which the difference is greater but there is no consistency in terms of which of the two is larger.

Composite First Motion Focal Mechanisms

The majority of the aftershocks are too small to be recorded outside of Haiti. However, there are not enough stations in Haiti to uniquely determine their focal mechanisms from first motion data. Instead, composite mechanisms are determined for these aftershocks. Composite mechanisms assume that nearby aftershocks occurred on the same fault segment and have the same focal mechanisms and that the data from them can therefore be combined and treated as a single earthquake (Sbar et al, 1972). If these criteria are not met, the resulting focal mechanism may be unreliable (Barth et al, 2008).

Because there was some indication from the mechanisms of the mainshock and largest aftershocks (Global CMT Project (2010)) that the style of faulting might not be uniform across the aftershock zone, the aftershocks were grouped into three geographical regions (Figure 3). The western region consists of earthquakes whose azimuth to the station JAKH is in the range of 105º-145º. The central group consists of earthquakes that are approximately due north of JAKH and north or west of LGNH. Earthquakes in the eastern region are also north of JAKH but to the east of LGNH. Whether the azimuth (earthquake to station) to LGNH is greater than or less than 200º determines which of these two groups the aftershocks are assigned to. Any events lying outside of these three regions were excluded. With eighty-

three polarity readings, the western group is the largest. The central and eastern groups have eighteen and twenty-three polarity readings respectively.

The first motions used were those recorded in the NEDB. There is a slight uncertainty in the azimuth to the station introduced by the choice of velocity model used to locate the earthquakes. A greater source of uncertainty, however, is associated with the take-off angle as it is dependent not only on the epicentral distance (velocity model dependent) but also on the depth of the earthquake. The depth is particularly of concern in this case since almost all of the phases used were Pg which is sensitive to depth whereas the take-off angle for Pn is independent of depth although it too will be affected by the choice of velocity model. The depths of most of the aftershocks were fixed at 10 km. A minimum magnitude (M_L) of 2.5 was used in the data selection to ensure that the phases read were likely to be clear. It has been verified (Bent, unpublished data) that the polarities of the instruments are correct.

The first motions were inverted for focal mechanism using the program "focmec" (Snoke et al, 1994), which is a grid search algorithm. While there were a number of misfits for each group, most of them were near nodal, suggesting that the composite solutions are a good approximation and that the misfits would likely be eliminated if the true depths of the earthquakes were known. The solutions were stable in the sense that as more aftershocks were added to the dataset, the focal mechanisms for each region did not change.

The resulting focal mechanisms were consistent geographically with the focal mechanisms of the mainshock and largest aftershock as determined from teleseismic data. That is, the western group was indicative of thrust faulting and the central and eastern groups of strike-slip faulting (Figure 5a-5c). It should be noted that the exact orientation of the strike-slip mechanism is not well-constrained. There are some polarities that misfit the preferred solution but they are near-nodal, suggesting that the exact mechanism for the earthquake from which the polarity was taken is slightly different from the average for the region or that the fixed depth (and therefore take-off angle) is incorrect.

Discussion and Conclusions

Individually determined focal mechanisms for the mainshock and moderate to large aftershocks of the 12 January 2010 Haiti earthquake and composite mechanisms for the smaller aftershocks suggest that the aftershock zone is dominated by strike-slip faulting in the east and thrust faulting in the west (Figure 6). The activity in the eastern zone is consistent with the expected style of faulting on the EPGF based on plate motion studies employing GPS as well as geological observations (Manaker et al, 2008; Mann et al, 1995, 2002). The thrust faulting in the west suggests that not all of the aftershocks are occurring on the EPGF but instead on what may be a landward extension of the South Haiti Fault and is referred to by Seeber and Waldhauser (2010) as the Jacmel thrust. Continued monitoring and analysis of the aftershock sequence and subsequent seismic activity in Haiti will provide additional data for verifying these conclusions and provide the backbone of future seismic hazard assessments for Haiti. For example, how much of the EPGF, if any, ruptured during the 2010 earthquake in still not known and which nearby faults may have ruptured also needs to be considered. While this paper was in review, a series of articles citing a wide range of seismological, geological and geophysical evidence were published (Calais et al, 2010; Hayes et al, 2010; Prentice et al, 2010) all of which concluded that little, and possibly

none, of the rupture associated with the 2010 earthquake occurred on the EPGF. Instead the rupture is believed to have occurred on a series of blind thrust faults with some strike-slip motion occurring at depth.

Acknowledgements

I thank John Adams for his constructive review. All maps were produced using the Generic Mapping Tool (GMT) of Wessel and Smith (1991). Waveform data were obtained from Natural Resources Canada and the IRIS Data Management Center.

References

Barth, A., J. Reinecker and O. Heidbach (2008). Stress derivation from earthquake focal mechanisms, *Guidelines: Focal Mechanisms*, World Stress Map Project, Potsdam, 8 p.

Bent, A. L., J. Drysdale, H. Greence, S. Halchuk, C. Woodgold, F. Proulx, D. A. McCormack, I. Al-Khoubbi, C. Andrews, I. Asudeh, D. Belizaire and H. Dorfeuuille (2010). Real Time Seismic Monitoring of Aftershocks of the 2010 Haiti Earthquake, paper accepted for presentation at the General Assembly of the European Seismological Commission, Sept. 2010, Montpellier, France.

Calais, E., A. Freed, G. Mattioli, F. Amelung, S. Jónsson, P. Jansma, S.-H. Hong, T. Dixon, C. Prépetit and R. Momplaisir (2010). Transpressional rupture of an unmapped fault during the 2010 Haiti earthquake, *Nature Geoscience*, **3**, 794-799, doi:10.1038/ngeo992.

Cassidy, J. F., I. Al-Khoubbi, G. C. Rogers, A. Bent, D. McCormack and C. Andrews (2010). New Observations of Earthquake Site Response and Seismic Attenuation in Haiti, *Seismological Research Letters*, **81**, 539.

Eberhard, M. O., S. Baldridge, J. Marshall, W. Mooney and G. J. Rix (2010). The Mw 7.0 Haiti earthquake of January 12, 2010; USGS/EERI Advance Reconnaissance Team Report, *U. S. Geological Survey Open-File Report 2010-1048*, 58 p.

Global CMT Project (2010). On-line database, http://www.globalcmt.org .

Hayes, G. P., R. W. Briggs, A. Sladen, E. J. Fielding, C. Prentice, K. Hudnut, P. Mann, F. W. Taylor, A. J. Crone, R. Gold, T. Ito and M. Simons (2010). Complex rupture during the 12 January 2010 Haiti earthquake, *Nature Geoscience*, **3**, 800-805, doi:10.1038/ngeo977.

Hjorleifsdöttir, V. and M. Nettles (2010). Source Mechanisms of the January 12, 2010 M_W 7.0 Haiti Earthquake and its Aftershocks, *Seismological Research Letters*, **81**, 542.

Huerfano, V. and K. Bataille (1994). Crustal structure and stress regime near Puerto Rico, in *Seismic Bulletin: Preliminary Locations of Earthquakes Recorded Near Puerto Rico*, January-December 1994, University of Puerto Rico at Mayagüez.

Kao, H., P.-R. Jiang, K.-F. Ma, B.-S. Huang and C.-C. Liu (1998). Moment-tensor inversion for offshore earthquakes east of Taiwan and their implications for regional collision, *Geophysical Research Letters*, **25**, 3619-3622.

Lin, J., R. S. Stein, V. Sevilgen and S. Toda (2010). USGS-WHOI-DPRI Coulomb Stress-Transfer Model for the January 12, 2010, M_W 7.0 Haiti Earthquake, *U. S. Geological Survey Open-File Report 2010-1019*, 7 p.

Manaker, D. M., E. Calais, A. M. Freed, S. T. Ali, P. Przybylski, G. Mattioli, P. Jansma, C. Prépetit and J. B. de Chabalier (2008). *Geophysical Journal International*, **174**, 889-903, doi:10.1111/j.1365-246X.2008.03819.x.

Mann, P., F. W. Taylor, R. L. Edwards and T.-L. Ku (1995). Actively evolving microplate formation by oblique collision and sideways motion along strike-slip faults: An example from the northeastern Caribbean plate margin, *Tectonophysics*, **246**, 1-69.

Mann, P., E. Calais, J.-C. Ruegg, C. DeMets, P. E. Jansma and G. S. Mattioli (2002). Oblique collision in the northeastern Caribbean from GPS measurements and geological observations, *Tectonics*, **21**, 7-1 – 7-23, doi:10.1029/2001TC001304.

McCormack, D. A., I. Al-Khoubbi, C. Andrews, I. Asudeh, M. Lamontagne, A. L. Bent, H. Greene, S. Halchuk, J. Drysdale, C. Woodgold and J. Adams (2010). Real Time Seismic Monitoring in Haiti, *Seismological Research Letters*, **81**, 540.

National Earthquake Database (2010). Digital database, http://www.seismo.nrcan.gc.ca Geological Survey of Canada, Ottawa, Ontario.

Prentice, C. S., P. Mann, A. J. Crone, R. D. Gold, K. W. Hudnut, R. W. Briggs, R. D. Keohler and P. Jean (2010). Seismic hazard of the Enriquillo-Plaintain Garden fault in haiti inferred from palaeoseismology, *Nature Geoscience*, **3**, 789-793, doi:10.1038/ngeo991.

Sbar, M. L., M. Barazangi, J. Dorman, C. H. Scholz and R. B. Smith (1972). Tectonics of the Intermountain Seismic Belt, western united States, Microearthquake seismicity and composite fault plane solutions, *Geological Society of America Bulletin*, **83**, 13-28.

Seeber, N. and F. Waldhauser (2010). The January 2010 Haiti Mainshock-Aftershock Discrepancy: Structural and Stress Interactions Between Faults in Strain Partitioned Transpression, *Seismological Research Letters*, **81**, 542.

Snoke, J. A., J. W. Munsey, A. G. Teague and G. A. Bollinger (1994). A program for focal mechanism determination by combined use of polarity and SV-P amplitude data (abstract), *Earthquake Notes*, **55(3)**, 15.

United States Geological Survey (2010). On-line database, http://neic.usgs.gov , United States Geological Survey, Golden, Colorado.

Waldhauser, F., N. Seeber, V. Hjorleifsdottir amd M. Nettles (2010). High-Resolution Aftershock Relocations and Focal Mechanisms of the 2010 M_W 7.0 Haiti and M_W 8.8 Chile Earthquakes, *Seismological Research Letters*, **81**, 543-544.

Wessel, P. and W. H. F. Smith (1991). Free software helps map and display data, *EOS, Transactions of the American Geophysical Union*, **72**, 441, 445-446.

Table
Aftershocks for Regional Moment Tensor Inversion

Date(yyyymmdd)	Time (hhmm, UT)	Lat. (ºN)	Lon. (ºW)	m_b	M_W	Depth (km)
20100113	2126	18.49	72.50	4.9	4.96	2
20100113	2221	18.36	72.58	4.9	4.87	15
20100114	1239	18.38	72.74	4.8	4.86	5
20100115	2104	18.12	72.30	4.7	4.83	2
20100116	1559	18.05	72.37	4.4	4.71	5
20100124	2151	18.51	72.64	4.5	4.41	10
20100126	1116	18.52	72.98	4.5	4.37	10
20100127	0057	18.37	72.85	4.8	4.81	6
20100204	0500	18.53	72.77	4.6	4.05	6
20100222	0936	18.49	72.56	4.6	4.62	8
20100223	0626	18.43	72.61	4.8	4.67	8
20100301	1037	18.44	72.75	4.6	4.29	5
20100520	0634	18.42	72.76	4.5	4.19	6

Note: M_W and depth are the values obtained in this study. All other parameters in the Table are from the USGS (2010).

Figures

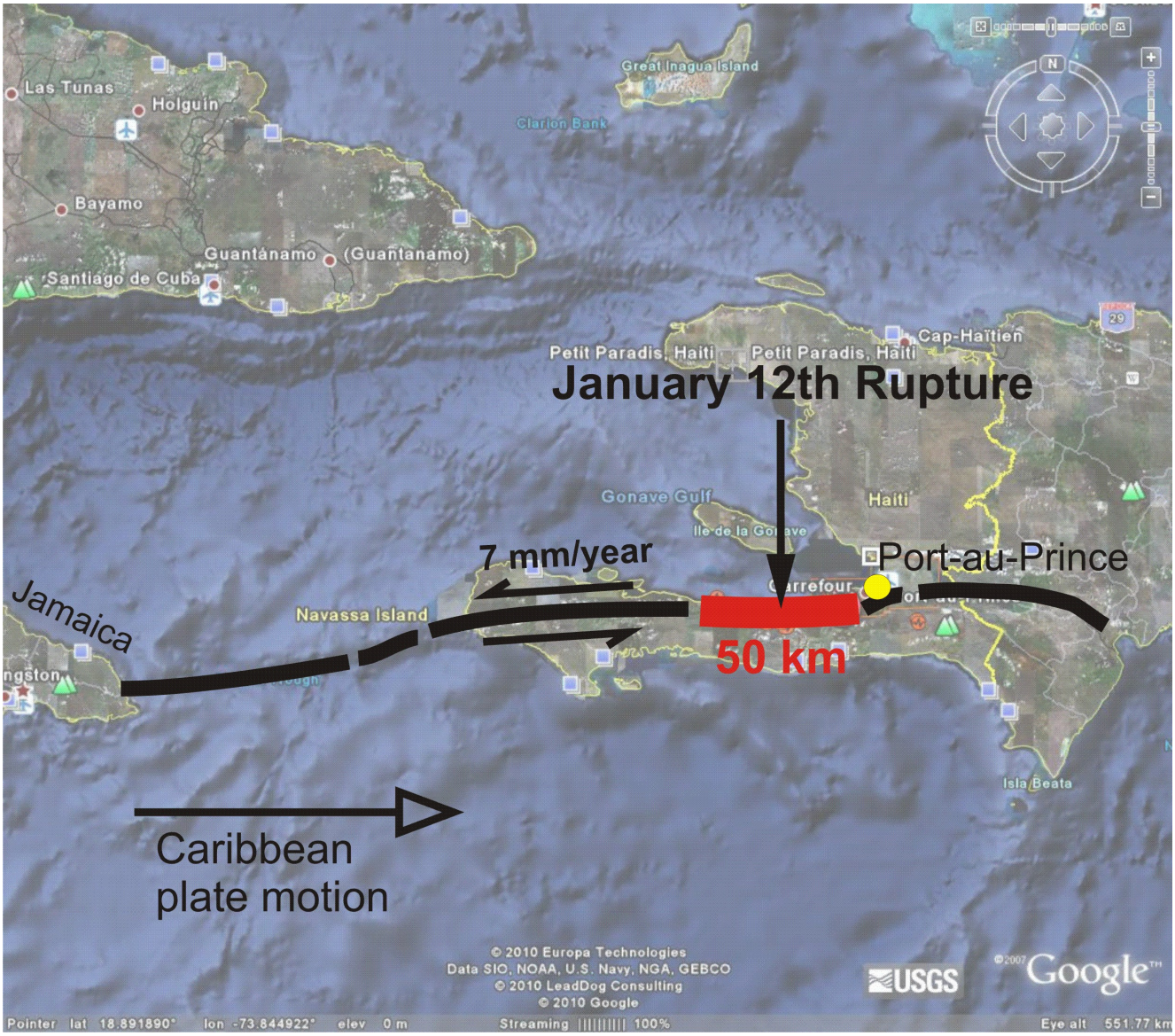

Figure 1. Map showing the Enriquillo-Plaintain Garden Fault zone (black) with the segment that ruptured during the 12 January 2010 earthquake highlighted in red. The relative motion between the North American and Caribbean plates is also shown. USGS/Google (2010) map with annotations by J. Adams.

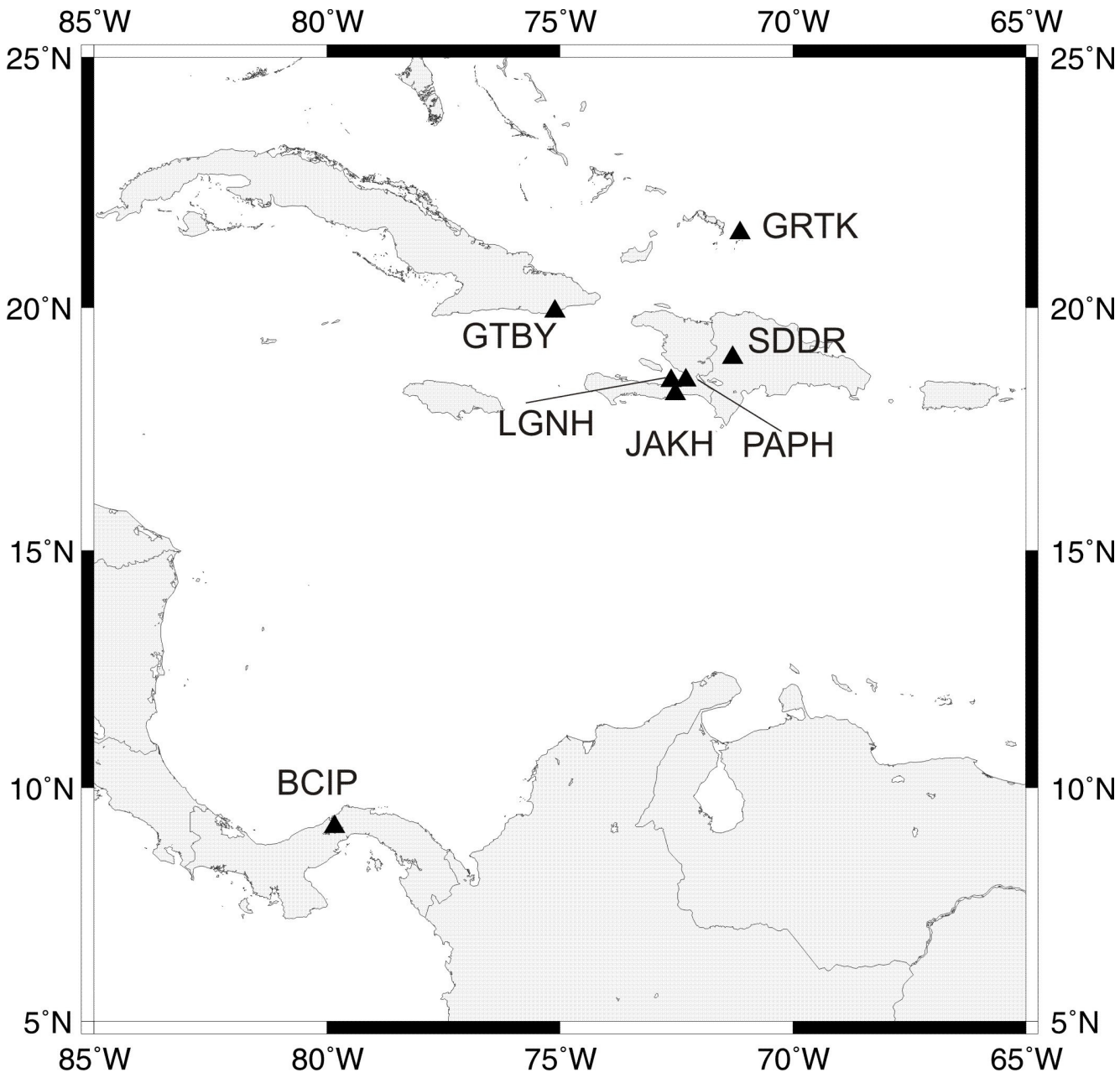

Figure 2: Stations used for focal mechanisms determined in this study.

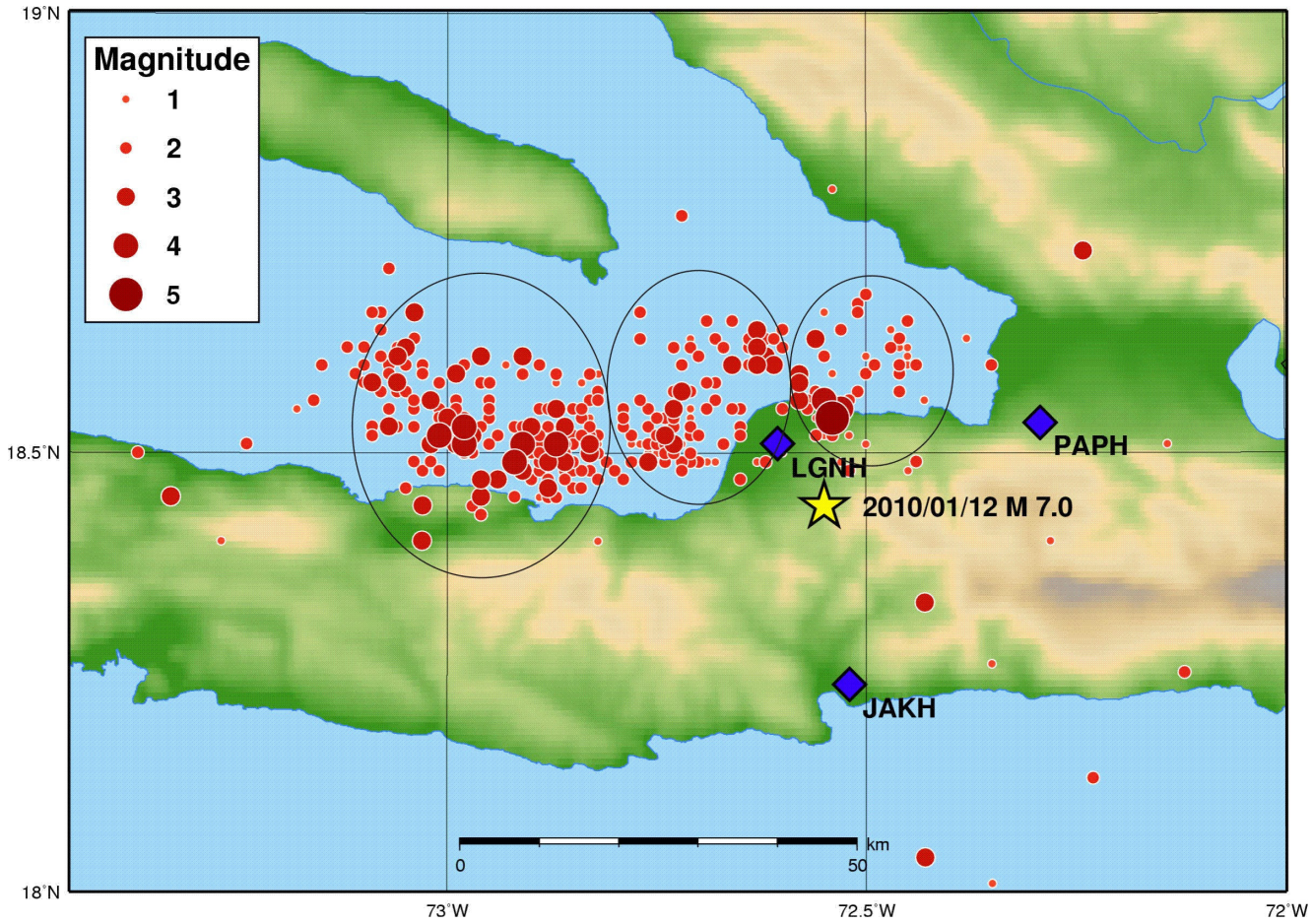

Figure 3: Aftershocks located by the Geological Survey of Canada from 15 February 2010 through 8 April 2010. The large circles show the approximate groupings used in the composite first motion solutions discussed in the text. Map drafted by S. Halchuk.

Figures 4a-4m: Regional moment tensor solutions for selected aftershocks. For each station the first line of text indicates the frequencies modeled (selected by the inversion program within a range of predefined values), the second gives the station code, distance (km) and azimuth (degrees), and the third indicates the velocity model used (Huerfano and Bataille, 1994 in all cases) and the weighting of each component. Note that the misfit is calculated for all components whether or not they are used in the inversion. The dark lines are the data and the lighter lines are the synthetic seismograms. The numbers next to each data-synthetic pair indicate the amplitude relative to the largest component and the misfit. The preferred solution is in the upper right corner with the inset showing the misfit as a function of depth.

Figure 4a

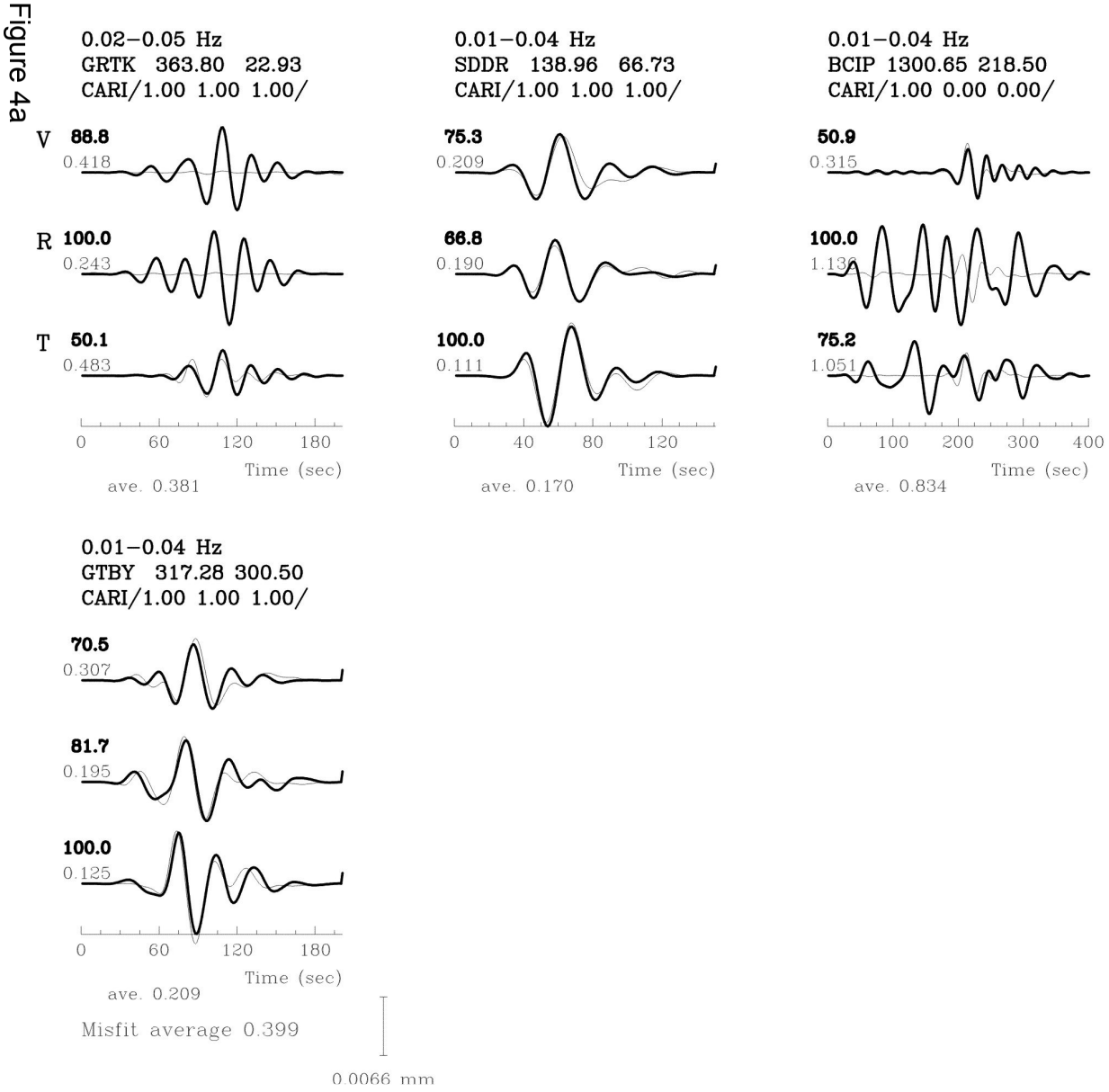
0.02–0.05 Hz
GRTK 363.80 22.93
CARI/1.00 1.00 1.00/
V 88.8
0.418
R 100.0
0.243
T 50.1
0.483
0 60 120 180
Time (sec)
ave. 0.381
0.01–0.04 Hz
SDDR 138.96 66.73
CARI/1.00 1.00 1.00/
75.3
0.209
66.8
0.190
100.0
0.111
0 40 80 120
Time (sec)
ave. 0.170
0.01–0.04 Hz
BCIP 1300.65 218.50
CARI/1.00 0.00 0.00/
50.9
0.315
100.0
1.136
75.2
1.051
0 100 200 300 400
Time (sec)
ave. 0.834
0.01–0.04 Hz
GTBY 317.28 300.50
CARI/1.00 1.00 1.00/
70.5
0.307
81.7
0.195
100.0
0.125
0 60 120 180
Time (sec)
ave. 0.209
Misfit average 0.399
0.0066 mm

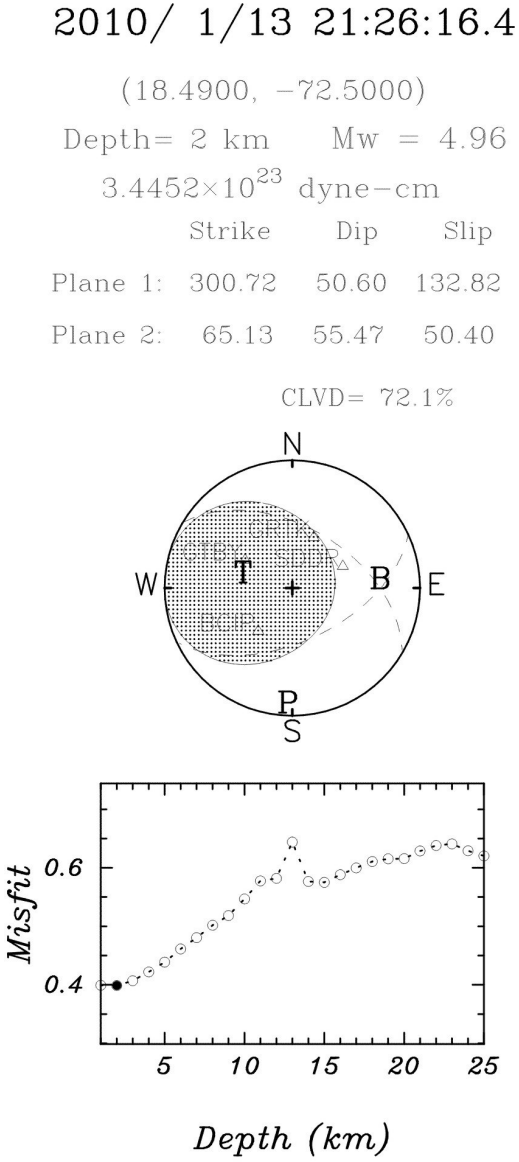
2010/ 1/13 21:26:16.4
(18.4900, −72.5000)
Depth= 2 km Mw = 4.96
3.4452×10^23 dyne−cm
Strike Dip Slip
Plane 1: 300.72 50.60 132.82
Plane 2: 65.13 55.47 50.40
CLVD= 72.1%
N
W
E
S
T
B
P
Misfit
0.6
0.4
5 10 15 20 25
Depth (km)

Figure 4b

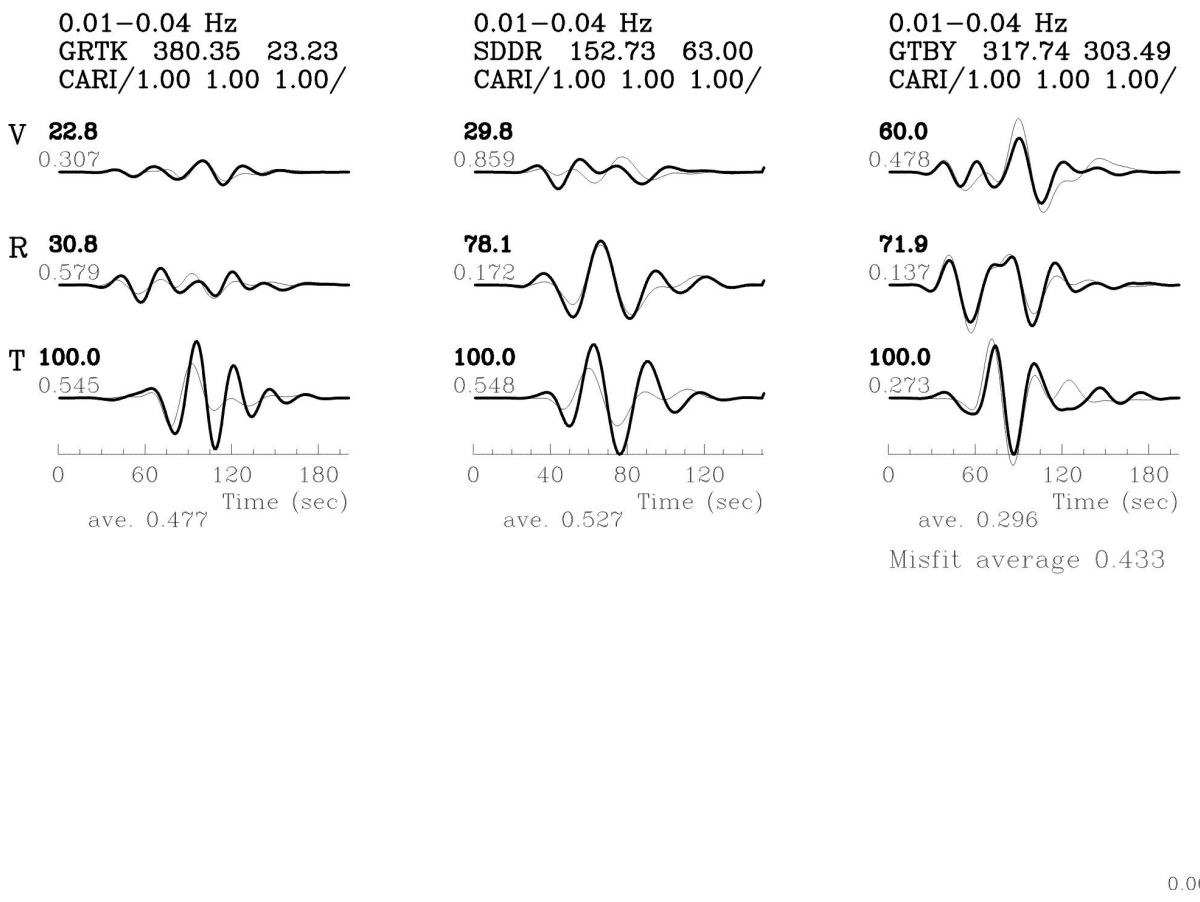
0.01−0.04 Hz
GRTK 380.35 23.23
CARI/1.00 1.00 1.00/
V 22.8
0.307
R 30.8
0.579
T 100.0
0.545
0 60 120 180
Time (sec)
ave. 0.477
0.01−0.04 Hz
SDDR 152.73 63.00
CARI/1.00 1.00 1.00/
29.8
0.859
78.1
0.172
100.0
0.548
0 40 80 120
Time (sec)
ave. 0.527
0.01−0.04 Hz
GTBY 317.74 303.49
CARI/1.00 1.00 1.00/
60.0
0.478
71.9
0.137
100.0
0.273
0 60 120 180
Time (sec)
ave. 0.296
Misfit average 0.433
2010/ 1/13 22:21:13.3
(18.3600, −72.5800)
Depth= 15 km Mw = 4.87
2.5024×10^23 dyne−cm
Strike Dip Slip
Plane 1: 45.99 34.81 72.53
Plane 2: 246.96 57.01 101.79
CLVD= 9.3%
N
P
GRTK△
GTBY△
B
W
T
E
S
Misfit
0.6
0.4
5 10 15 20 25
Depth (km)
0.0035 mm

Figure 4c

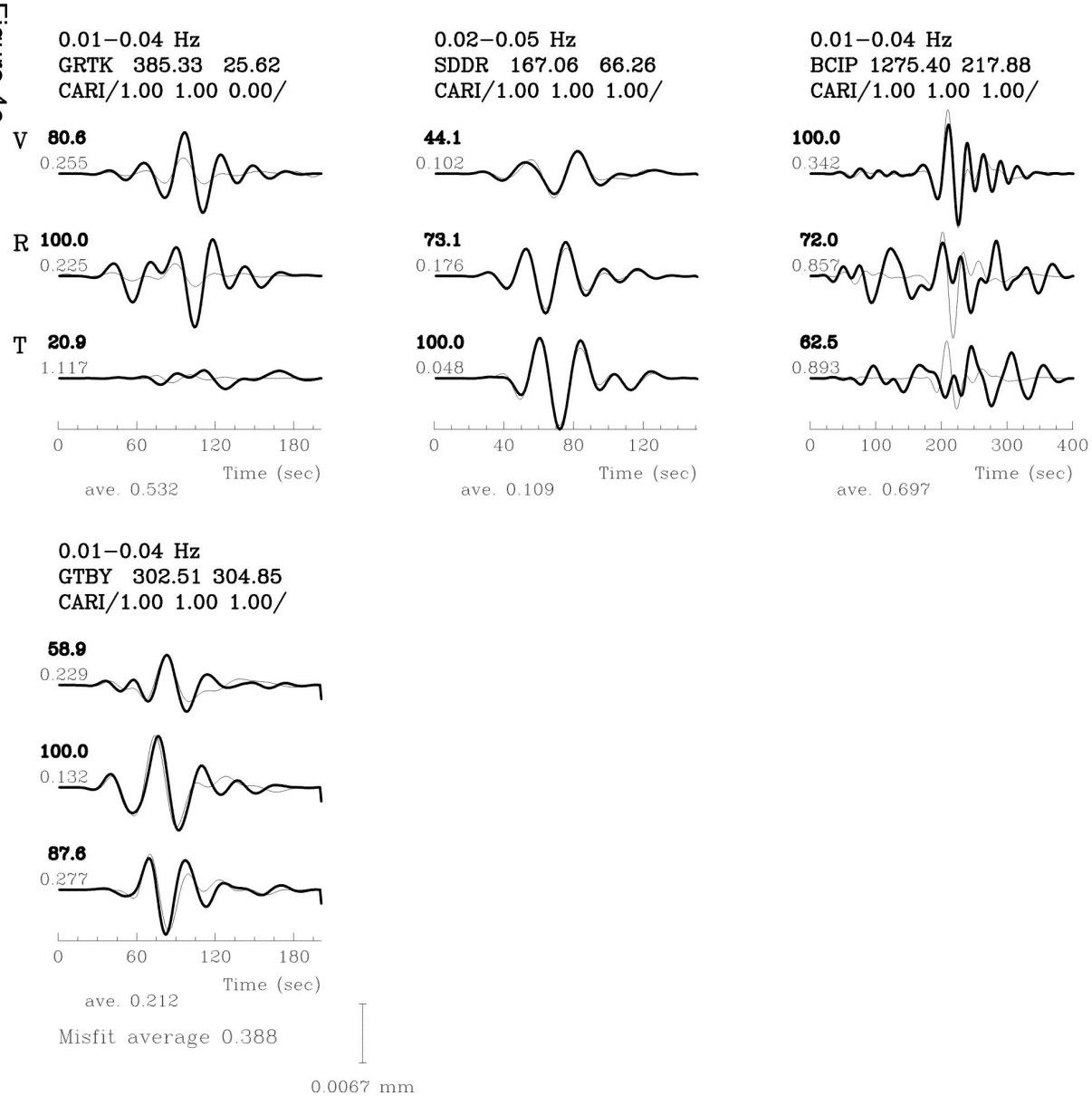
0.01−0.04 Hz
GRTK 385.33 25.62
CARI/1.00 1.00 0.00/
V 80.6
0.255
R 100.0
0.225
T 20.9
1.117
0 60 120 180
Time (sec)
ave. 0.532
0.02−0.05 Hz
SDDR 167.06 66.26
CARI/1.00 1.00 1.00/
44.1
0.102
73.1
0.176
100.0
0.048
0 40 80 120
Time (sec)
ave. 0.109
0.01−0.04 Hz
BCIP 1275.40 217.88
CARI/1.00 1.00 1.00/
100.0
0.342
72.0
0.857
62.5
0.893
0 100 200 300 400
Time (sec)
ave. 0.697
0.01−0.04 Hz
GTBY 302.51 304.85
CARI/1.00 1.00 1.00/
58.9
0.229
100.0
0.132
87.6
0.277
0 60 120 180
Time (sec)
ave. 0.212
Misfit average 0.388
0.0067 mm

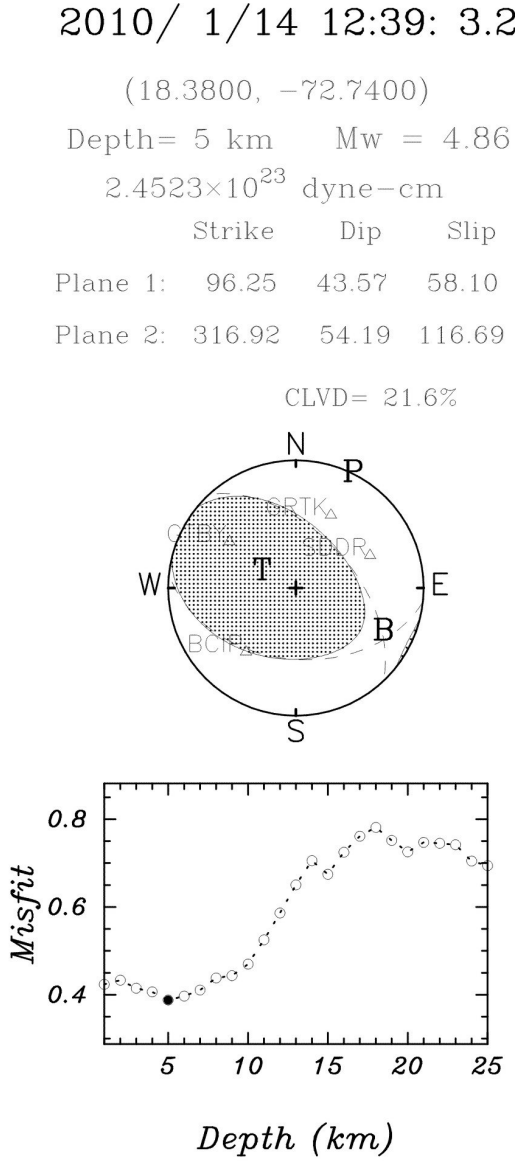
2010/ 1/14 12:39: 3.2
(18.3800, −72.7400)
Depth= 5 km Mw = 4.86
2.4523×10^23 dyne−cm
Strike Dip Slip
Plane 1: 96.25 43.57 58.10
Plane 2: 316.92 54.19 116.69
CLVD= 21.6%
N
P
W
E
T
B
S
GRTK
SDDR
BCIP
Misfit
0.8
0.6
0.4
5 10 15 20 25
Depth (km)

Figure 4d

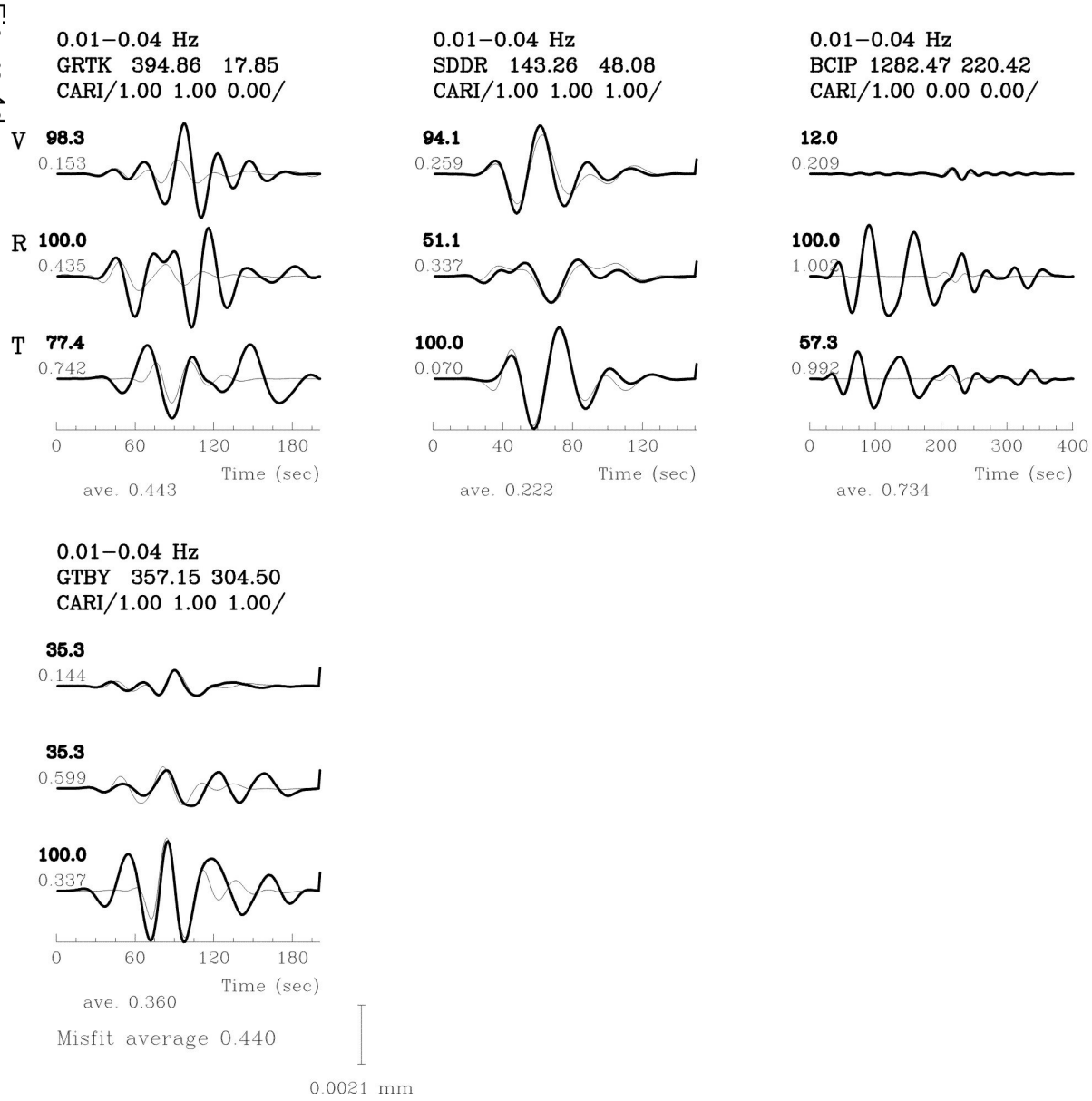
0.01−0.04 Hz
GRTK 394.86 17.85
CARI/1.00 1.00 0.00/
V 98.3
0.153
R 100.0
0.435
T 77.4
0.742
0 60 120 180
Time (sec)
ave. 0.443
0.01−0.04 Hz
SDDR 143.26 48.08
CARI/1.00 1.00 1.00/
94.1
0.259
51.1
0.337
100.0
0.070
0 40 80 120
Time (sec)
ave. 0.222
0.01−0.04 Hz
BCIP 1282.47 220.42
CARI/1.00 0.00 0.00/
12.0
0.209
100.0
1.002
57.3
0.992
0 100 200 300 400
Time (sec)
ave. 0.734
0.01−0.04 Hz
GTBY 357.15 304.50
CARI/1.00 1.00 1.00/
35.3
0.144
35.3
0.599
100.0
0.337
0 60 120 180
Time (sec)
ave. 0.360
Misfit average 0.440
0.0021 mm

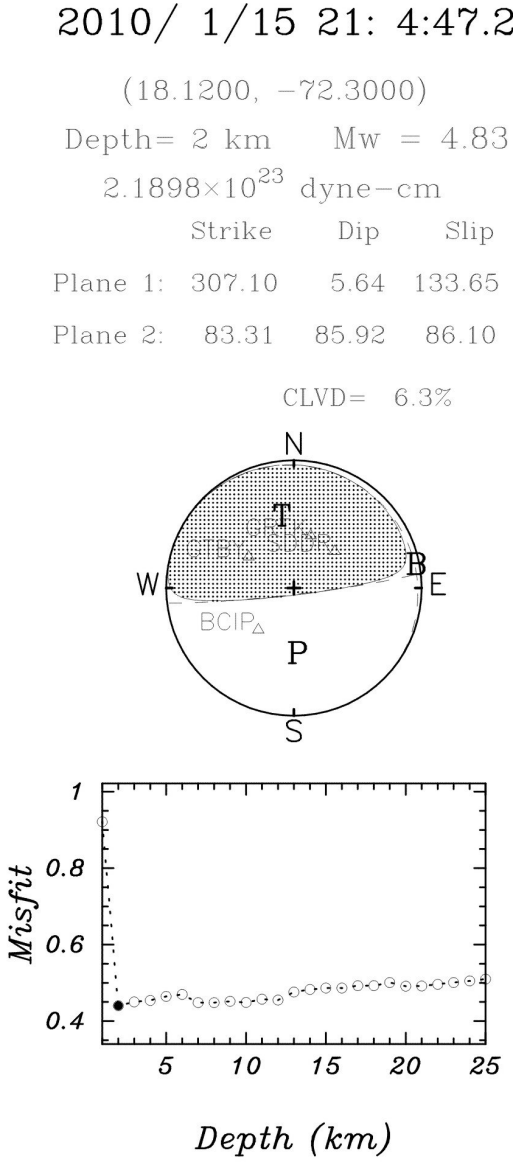
2010/ 1/15 21: 4:47.2
(18.1200, −72.3000)
Depth= 2 km Mw = 4.83
2.1898×10^23 dyne−cm
Strike Dip Slip
Plane 1: 307.10 5.64 133.65
Plane 2: 83.31 85.92 86.10
CLVD= 6.3%
N
W
E
S
T
P
B
BCIP△
1
0.8
0.6
0.4
Misfit
5 10 15 20 25
Depth (km)

Figure 4e

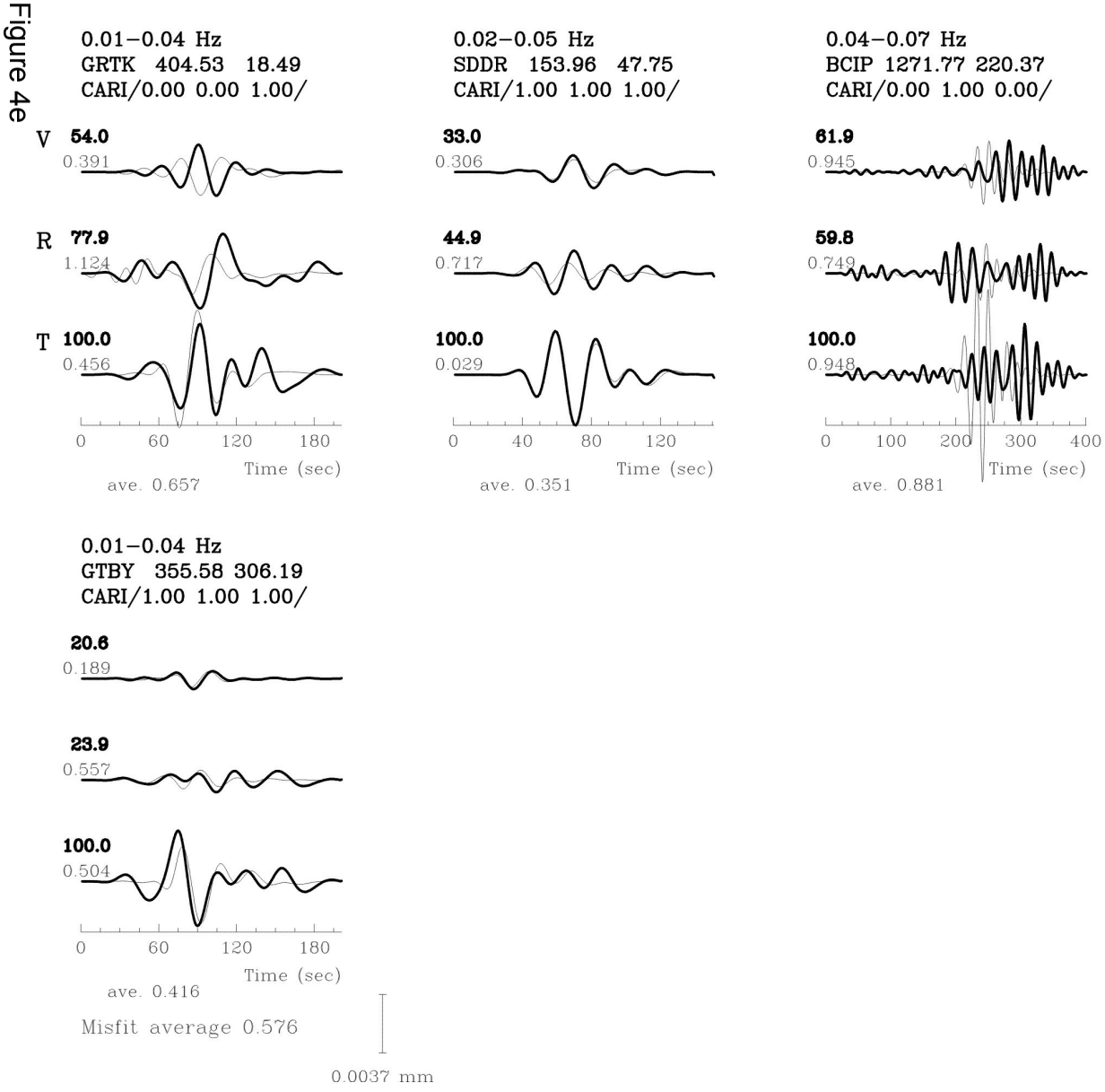
0.01−0.04 Hz
GRTK 404.53 18.49
CARI/0.00 0.00 1.00/
V 54.0
0.391
R 77.9
1.124
T 100.0
0.456
0 60 120 180
Time (sec)
ave. 0.657
0.02−0.05 Hz
SDDR 153.96 47.75
CARI/1.00 1.00 1.00/
33.0
0.306
44.9
0.717
100.0
0.029
0 40 80 120
Time (sec)
ave. 0.351
0.04−0.07 Hz
BCIP 1271.77 220.37
CARI/0.00 1.00 0.00/
61.9
0.945
59.8
0.749
100.0
0.948
0 100 200 300 400
Time (sec)
ave. 0.881
0.01−0.04 Hz
GTBY 355.58 306.19
CARI/1.00 1.00 1.00/
20.6
0.189
23.9
0.557
100.0
0.504
0 60 120 180
Time (sec)
ave. 0.416
Misfit average 0.576
0.0037 mm

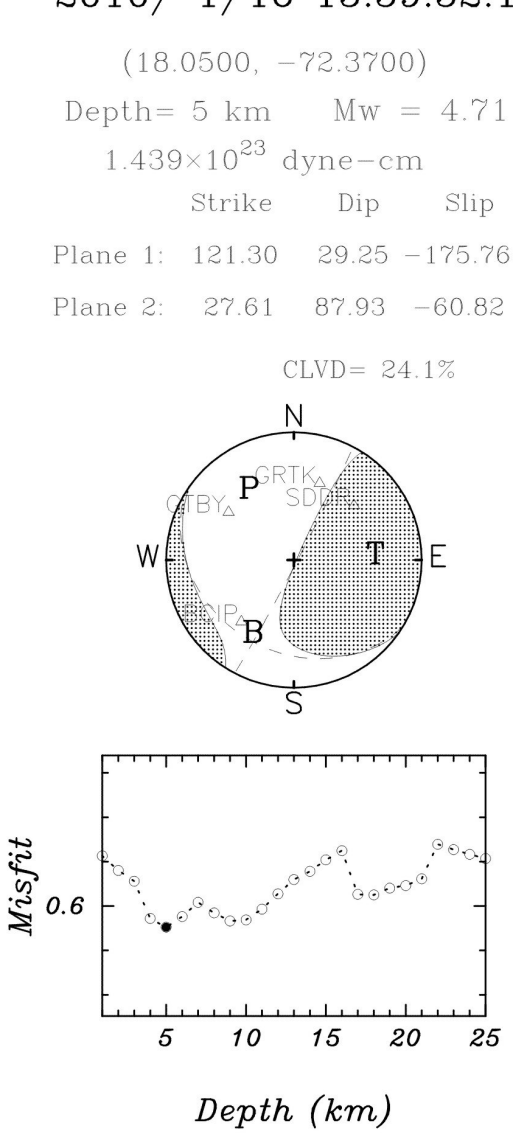
2010/ 1/16 15:59:52.1
(18.0500, −72.3700)
Depth= 5 km Mw = 4.71
1.439×10^23 dyne−cm
Strike Dip Slip
Plane 1: 121.30 29.25 −175.76
Plane 2: 27.61 87.93 −60.82
CLVD= 24.1%
N
W
E
S
P
T
B
GRTK
SDDR
GTBY
BCIP
Misfit
0.6
5 10 15 20 25
Depth (km)

Figure 4f

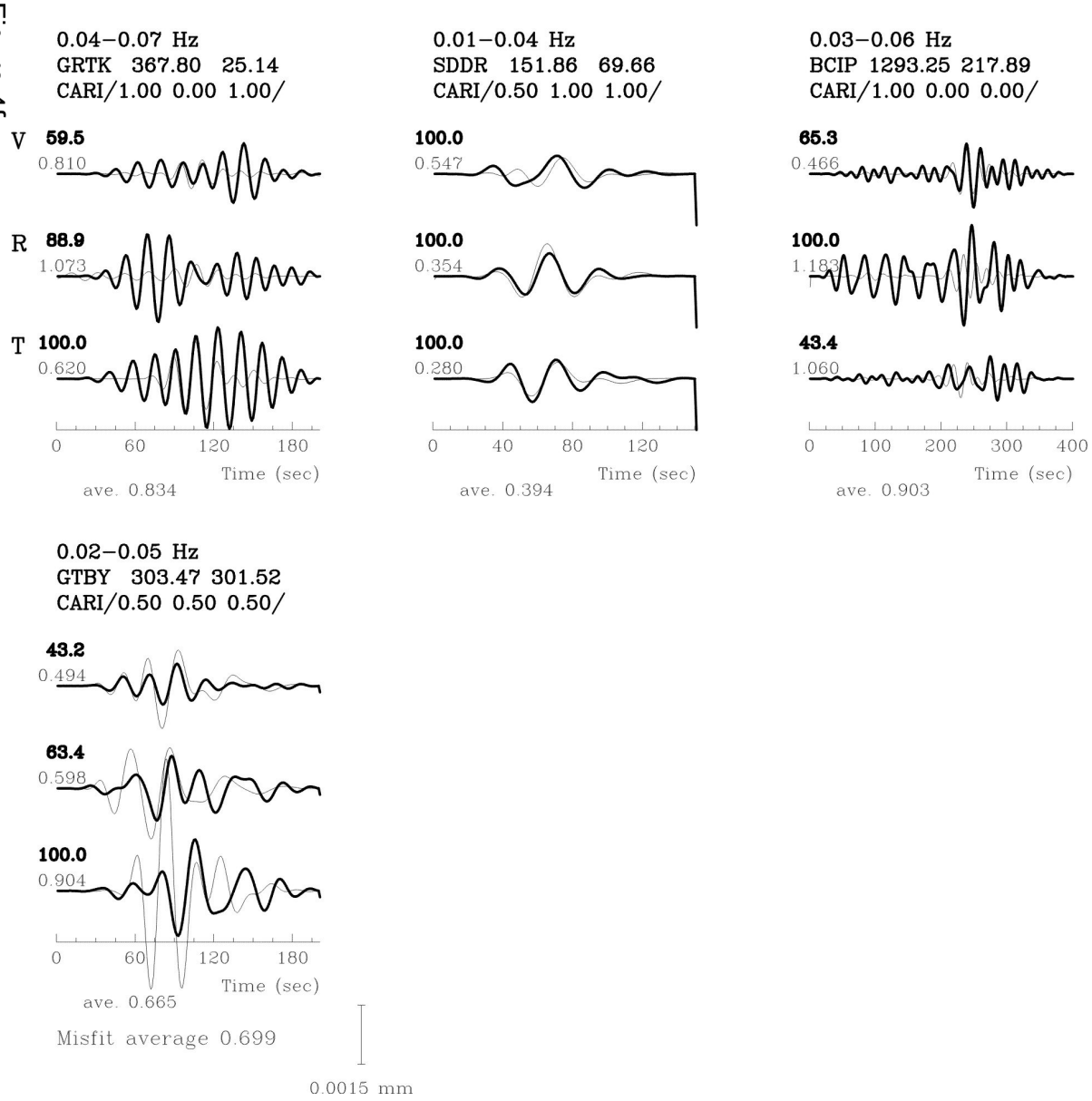
0.04–0.07 Hz
GRTK 367.80 25.14
CARI/1.00 0.00 1.00/
V 59.5
0.810
R 88.9
1.073
T 100.0
0.620
0 60 120 180
Time (sec)
ave. 0.834
0.01–0.04 Hz
SDDR 151.86 69.66
CARI/0.50 1.00 1.00/
100.0
0.547
100.0
0.354
100.0
0.280
0 40 80 120
Time (sec)
ave. 0.394
0.03–0.06 Hz
BCIP 1293.25 217.89
CARI/1.00 0.00 0.00/
65.3
0.466
100.0
1.183
43.4
1.060
0 100 200 300 400
Time (sec)
ave. 0.903
0.02–0.05 Hz
GTBY 303.47 301.52
CARI/0.50 0.50 0.50/
43.2
0.494
63.4
0.598
100.0
0.904
0 60 120 180
Time (sec)
ave. 0.665
Misfit average 0.699
0.0015 mm

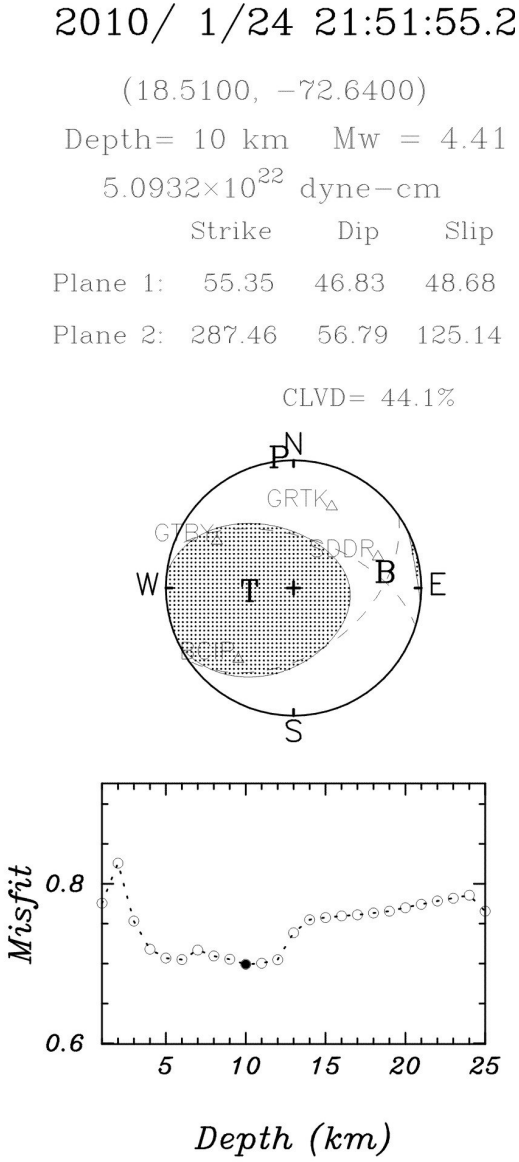
2010/ 1/24 21:51:55.2
(18.5100, −72.6400)
Depth= 10 km Mw = 4.41
5.0932×10^22 dyne−cm
Strike Dip Slip
Plane 1: 55.35 46.83 48.68
Plane 2: 287.46 56.79 125.14
CLVD= 44.1%
N
P
GRTK
GTBY
SDDR
W
T
B
E
S
Misfit
0.8
0.6
5 10 15 20 25
Depth (km)

Figure 4g

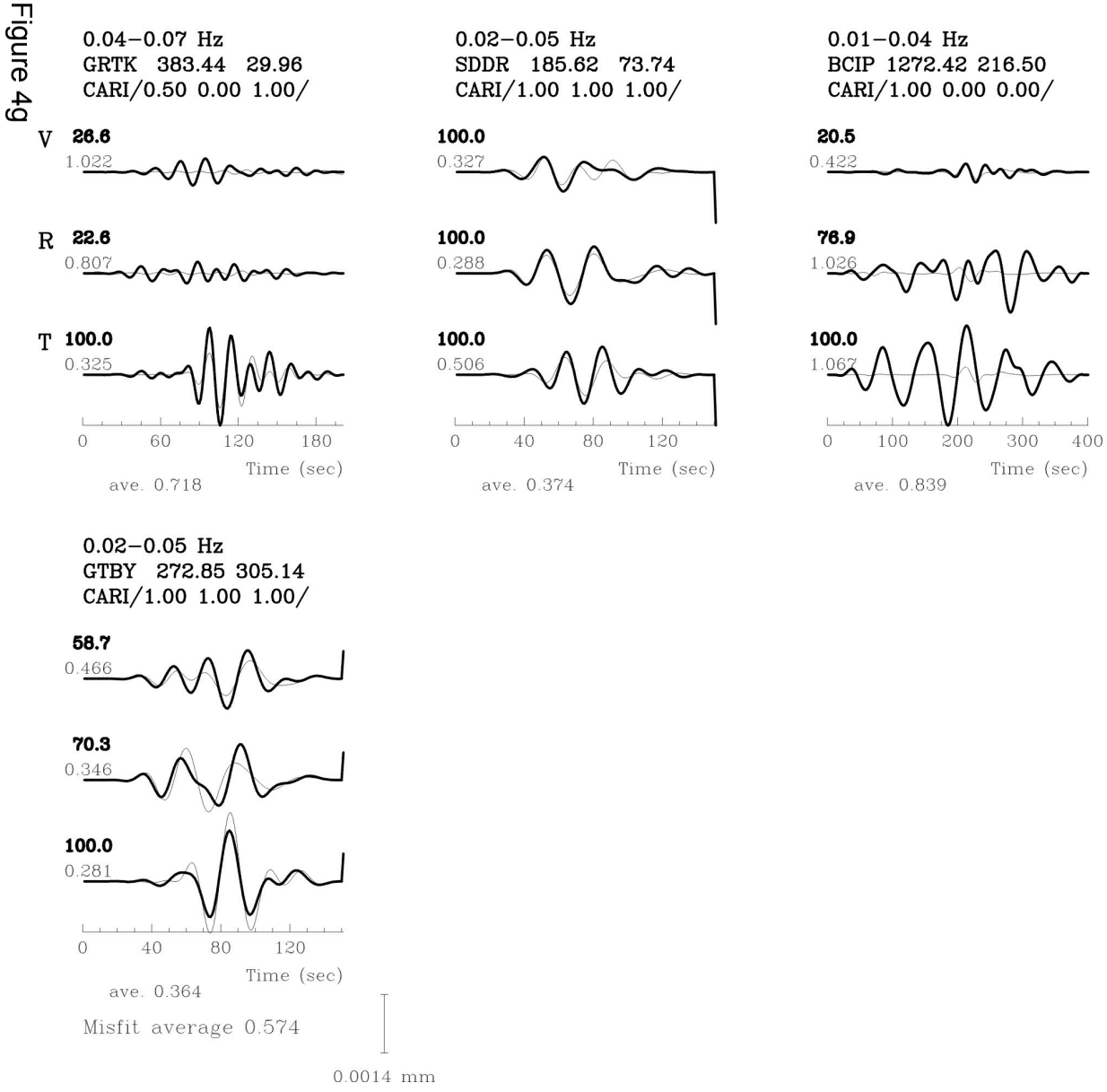
0.04–0.07 Hz
GRTK 383.44 29.96
CARI/0.50 0.00 1.00/
V 26.6
1.022
R 22.6
0.807
T 100.0
0.325
0 60 120 180
Time (sec)
ave. 0.718
0.02–0.05 Hz
SDDR 185.62 73.74
CARI/1.00 1.00 1.00/
100.0
0.327
100.0
0.288
100.0
0.506
0 40 80 120
Time (sec)
ave. 0.374
0.01–0.04 Hz
BCIP 1272.42 216.50
CARI/1.00 0.00 0.00/
20.5
0.422
76.9
1.026
100.0
1.067
0 100 200 300 400
Time (sec)
ave. 0.839
0.02–0.05 Hz
GTBY 272.85 305.14
CARI/1.00 1.00 1.00/
58.7
0.466
70.3
0.346
100.0
0.281
0 40 80 120
Time (sec)
ave. 0.364
Misfit average 0.574
0.0014 mm

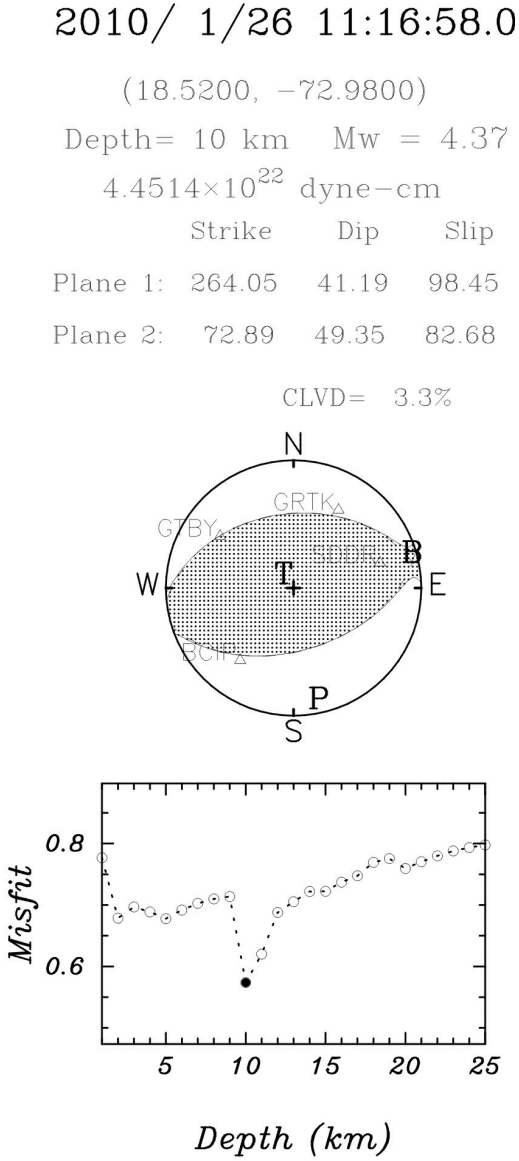
2010/ 1/26 11:16:58.0
(18.5200, −72.9800)
Depth= 10 km Mw = 4.37
4.4514×10^22 dyne-cm
Strike Dip Slip
Plane 1: 264.05 41.19 98.45
Plane 2: 72.89 49.35 82.68
CLVD= 3.3%
N
W
E
S
GRTK
GTBY
SDDR
BCIP
T
B
P
Misfit
0.8
0.6
5 10 15 20 25
Depth (km)

Figure 4h

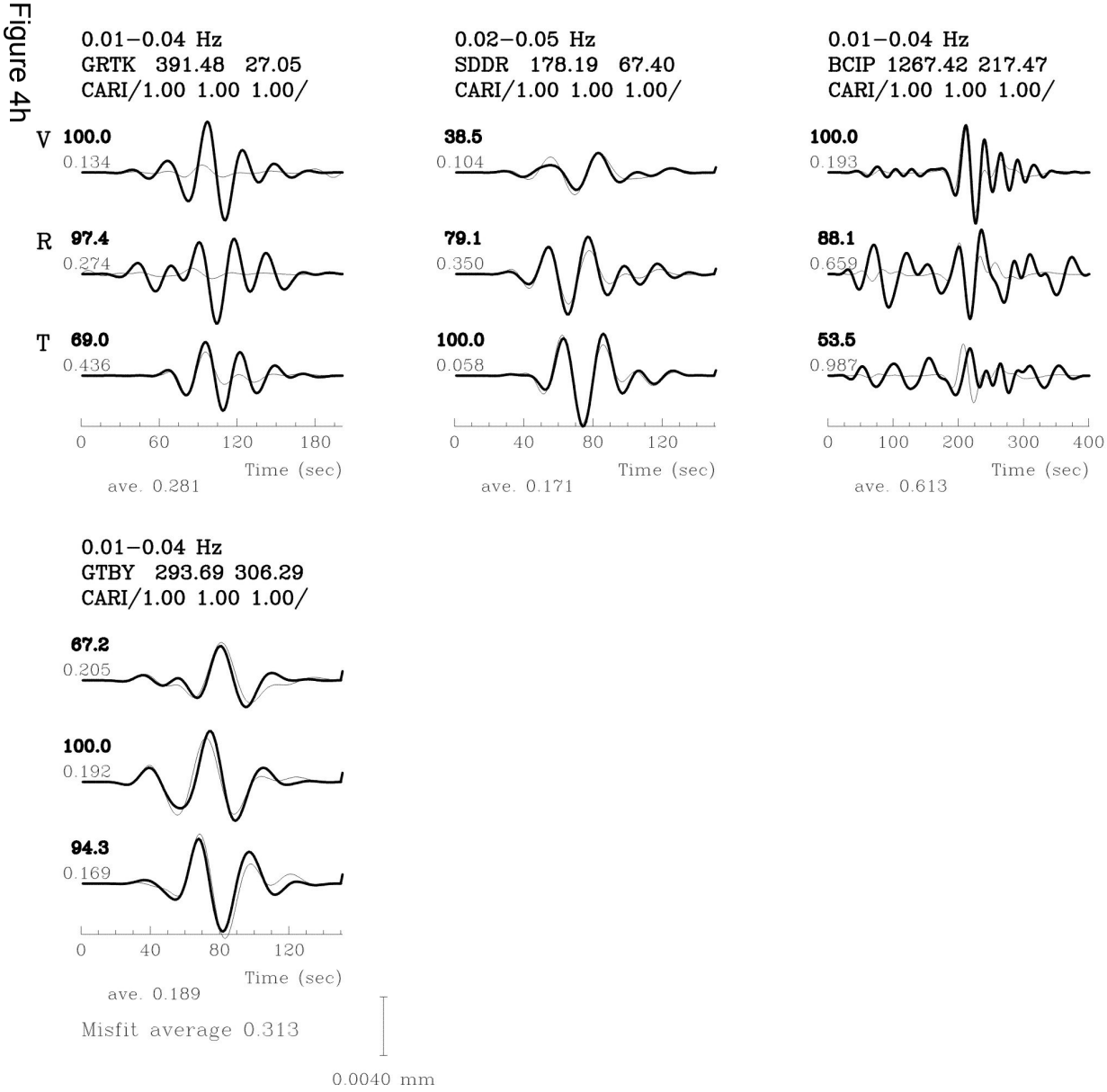
0.01–0.04 Hz
GRTK 391.48 27.05
CARI/1.00 1.00 1.00/
V 100.0
0.134
R 97.4
0.274
T 69.0
0.436
0 60 120 180
Time (sec)
ave. 0.281
0.02–0.05 Hz
SDDR 178.19 67.40
CARI/1.00 1.00 1.00/
38.5
0.104
79.1
0.350
100.0
0.058
0 40 80 120
Time (sec)
ave. 0.171
0.01–0.04 Hz
BCIP 1267.42 217.47
CARI/1.00 1.00 1.00/
100.0
0.193
88.1
0.659
53.5
0.987
0 100 200 300 400
Time (sec)
ave. 0.613
0.01–0.04 Hz
GTBY 293.69 306.29
CARI/1.00 1.00 1.00/
67.2
0.205
100.0
0.192
94.3
0.169
0 40 80 120
Time (sec)
ave. 0.189
Misfit average 0.313
0.0040 mm

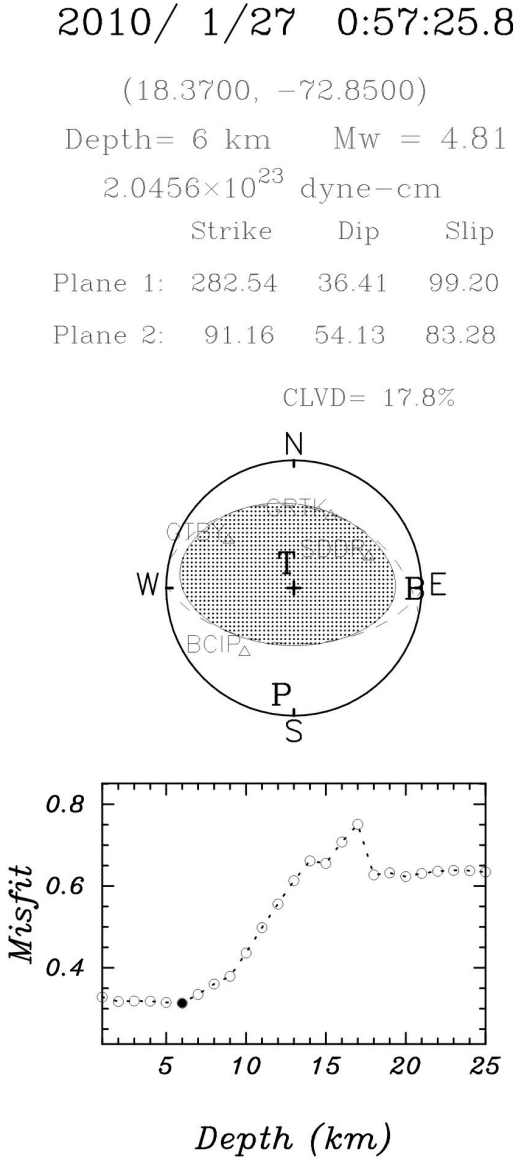
2010/ 1/27 0:57:25.8
(18.3700, −72.8500)
Depth= 6 km Mw = 4.81
2.0456×10^23 dyne-cm
Strike Dip Slip
Plane 1: 282.54 36.41 99.20
Plane 2: 91.16 54.13 83.28
CLVD= 17.8%
N
W
E
S
T
P
B
GRTK
CARI
SDDR
BCIP
Misfit
0.8
0.6
0.4
5 10 15 20 25
Depth (km)

Figure 4i

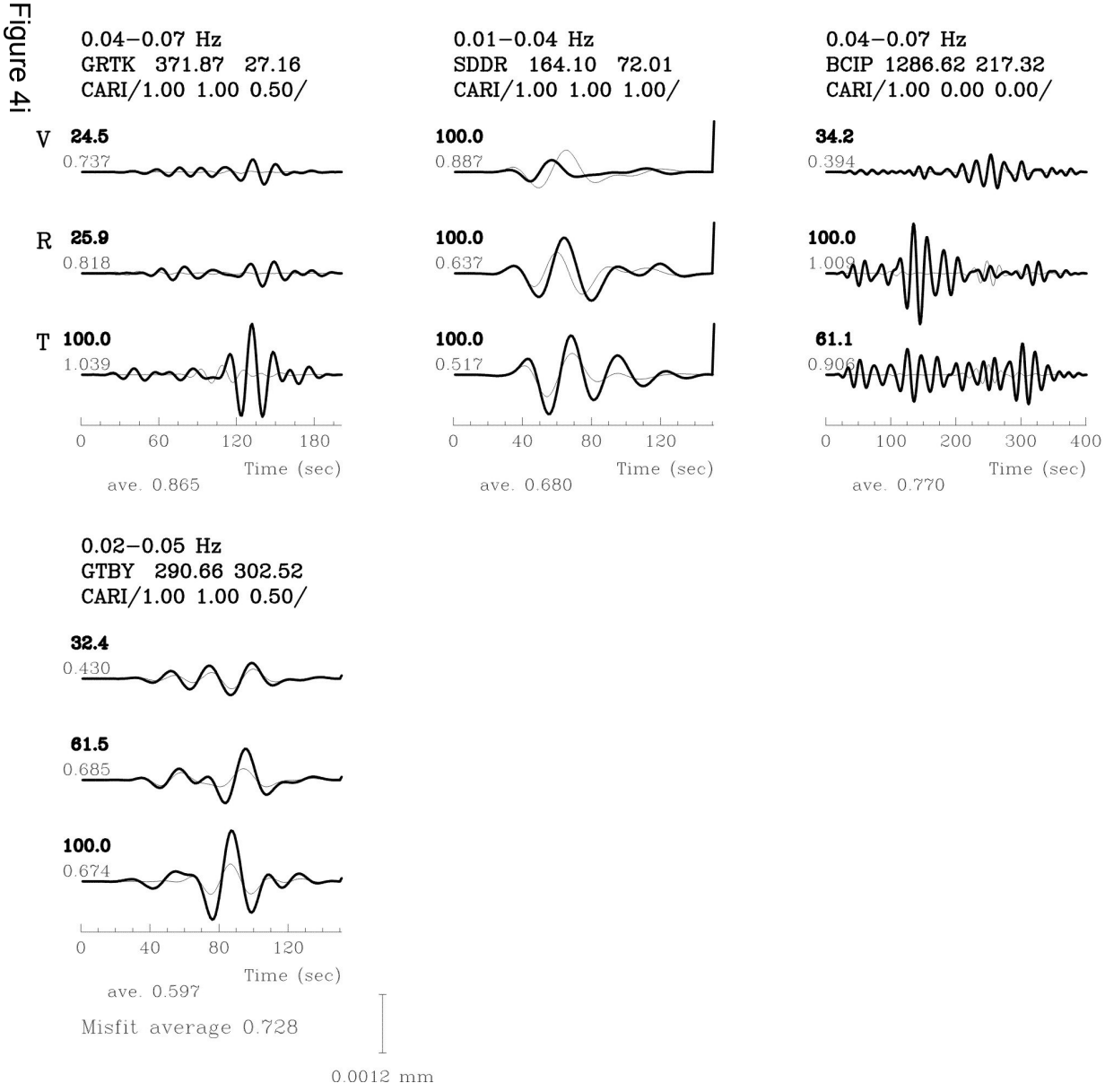
0.04–0.07 Hz
GRTK 371.87 27.16
CARI/1.00 1.00 0.50/
V 24.5
0.737
R 25.9
0.818
T 100.0
1.039
0 60 120 180
Time (sec)
ave. 0.865
0.01–0.04 Hz
SDDR 164.10 72.01
CARI/1.00 1.00 1.00/
100.0
0.887
100.0
0.637
100.0
0.517
0 40 80 120
Time (sec)
ave. 0.680
0.04–0.07 Hz
BCIP 1286.62 217.32
CARI/1.00 0.00 0.00/
34.2
0.394
100.0
1.009
61.1
0.906
0 100 200 300 400
Time (sec)
ave. 0.770
0.02–0.05 Hz
GTBY 290.66 302.52
CARI/1.00 1.00 0.50/
32.4
0.430
61.5
0.685
100.0
0.674
0 40 80 120
Time (sec)
ave. 0.597
Misfit average 0.728
0.0012 mm

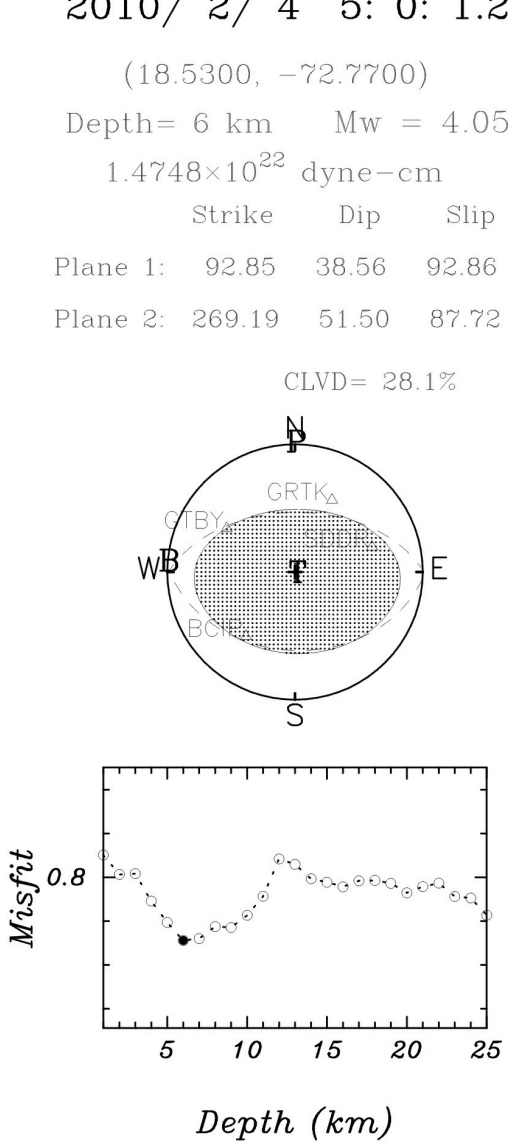
2010/ 2/ 4 5: 0: 1.2
(18.5300, −72.7700)
Depth= 6 km Mw = 4.05
1.4748×10^22 dyne−cm
Strike Dip Slip
Plane 1: 92.85 38.56 92.86
Plane 2: 269.19 51.50 87.72
CLVD= 28.1%
N
W
E
S
GRTK
GTBY
BCIP
SDDR
Misfit
0.8
5 10 15 20 25
Depth (km)

Figure 4j

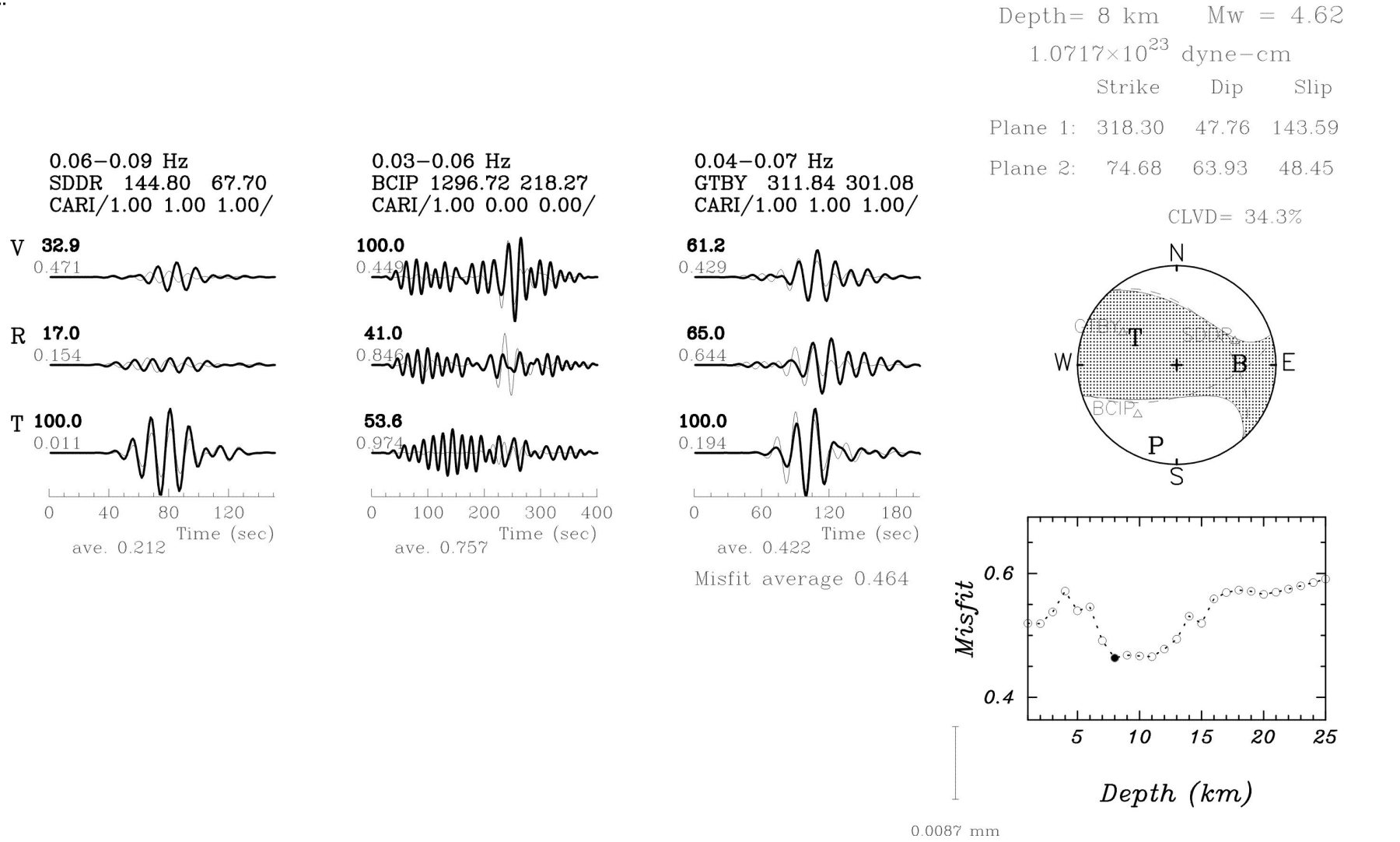
0.06−0.09 Hz
SDDR 144.80 67.70
CARI/1.00 1.00 1.00/
V 32.9
0.471
R 17.0
0.154
T 100.0
0.011
0 40 80 120
Time (sec)
ave. 0.212
0.03−0.06 Hz
BCIP 1296.72 218.27
CARI/1.00 0.00 0.00/
100.0
0.448
41.0
0.846
53.6
0.974
0 100 200 300 400
Time (sec)
ave. 0.757
0.04−0.07 Hz
GTBY 311.84 301.08
CARI/1.00 1.00 1.00/
61.2
0.429
65.0
0.644
100.0
0.194
0 60 120 180
Time (sec)
ave. 0.422
Misfit average 0.464
2010/ 2/22 9:36: 3.1
(18.4900, −72.5600)
Depth= 8 km Mw = 4.62
1.0717×10^23 dyne−cm
Strike Dip Slip
Plane 1: 318.30 47.76 143.59
Plane 2: 74.68 63.93 48.45
CLVD= 34.3%
N
W
E
S
T
B
P
BCIP
Misfit
0.6
0.4
5 10 15 20 25
Depth (km)
0.0087 mm

Figure 4k

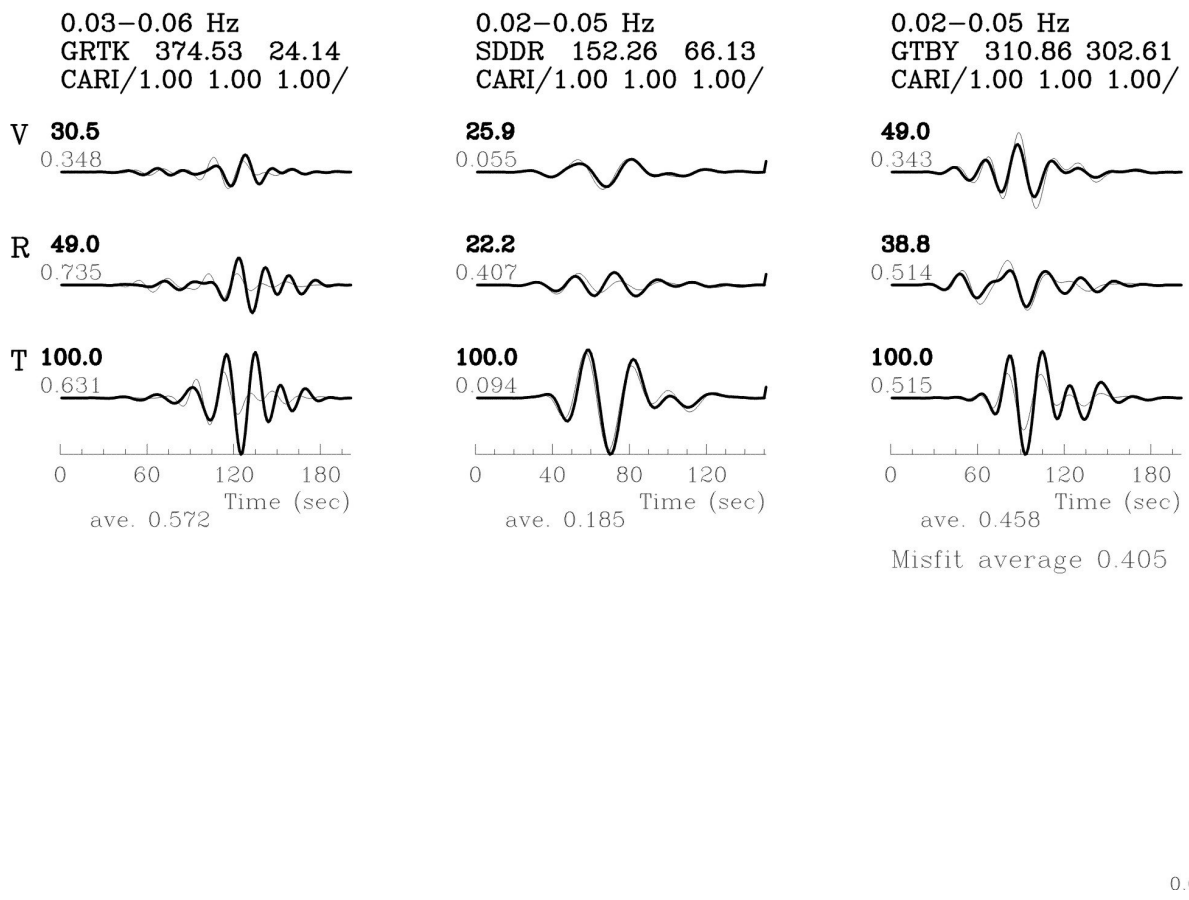
0.03–0.06 Hz
GRTK 374.53 24.14
CARI/1.00 1.00 1.00/
V 30.5
0.348
R 49.0
0.735
T 100.0
0.631
0 60 120 180
Time (sec)
ave. 0.572
0.02–0.05 Hz
SDDR 152.26 66.13
CARI/1.00 1.00 1.00/
25.9
0.055
22.2
0.407
100.0
0.094
0 40 80 120
Time (sec)
ave. 0.185
0.02–0.05 Hz
GTBY 310.86 302.61
CARI/1.00 1.00 1.00/
49.0
0.343
38.8
0.514
100.0
0.515
0 60 120 180
Time (sec)
ave. 0.458
Misfit average 0.405
2010/ 2/23 6:26:20.7
(18.4300, −72.6100)
Depth= 8 km Mw = 4.67
1.2452×10^23 dyne−cm
Strike Dip Slip
Plane 1: 171.76 53.25 171.63
Plane 2: 266.79 83.30 37.04
CLVD= 19.4%
N
P
GRTK△
CARI△
SDDR△
W
B
E
T
S
Misfit
0.6
0.4
5 10 15 20 25
Depth (km)
0.0044 mm

Figure 4l

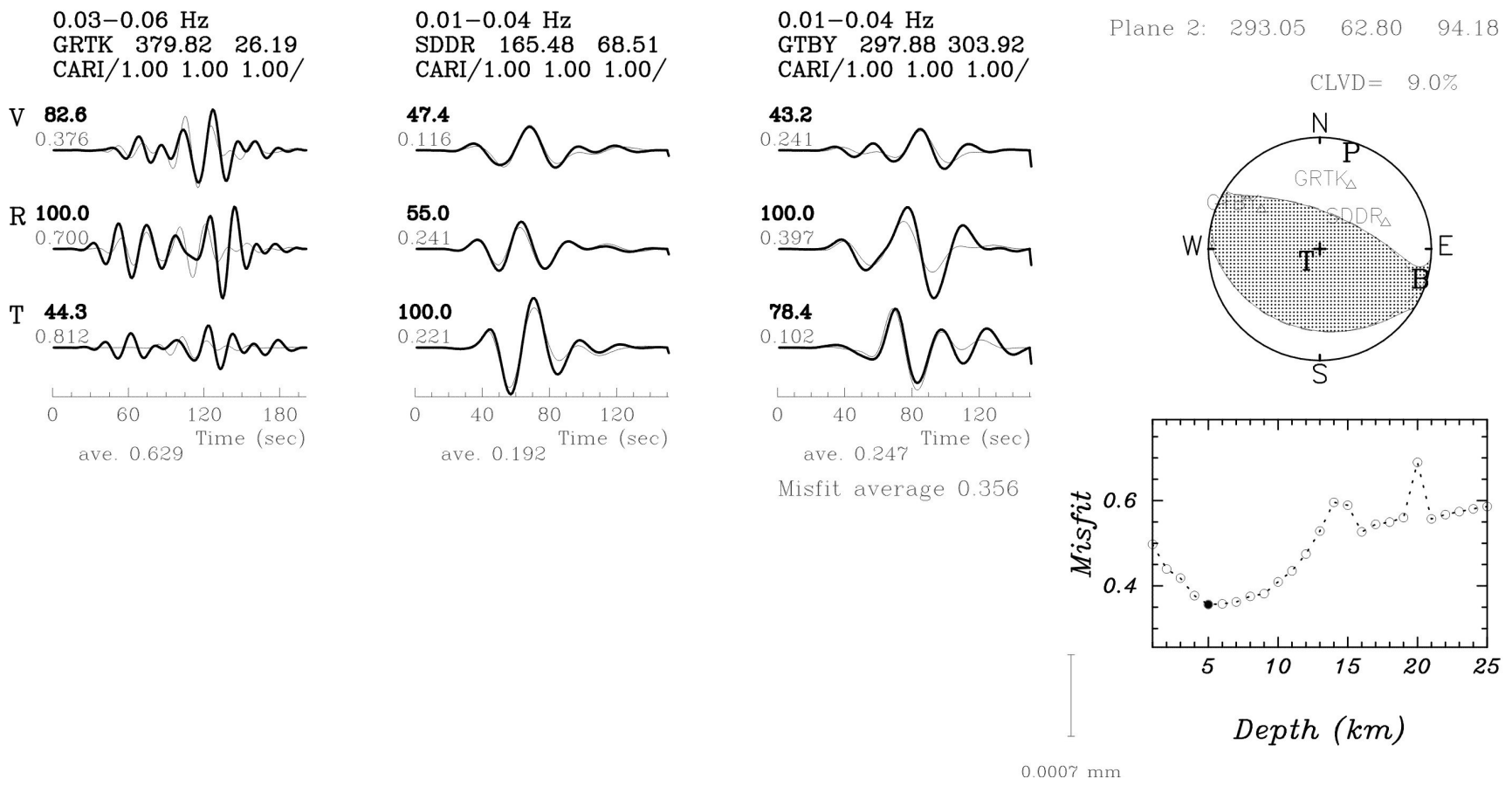
0.03−0.06 Hz
GRTK 379.82 26.19
CARI/1.00 1.00 1.00/
V 82.6
0.376
R 100.0
0.700
T 44.3
0.812
0 60 120 180
Time (sec)
ave. 0.629
0.01−0.04 Hz
SDDR 165.48 68.51
CARI/1.00 1.00 1.00/
47.4
0.116
55.0
0.241
100.0
0.221
0 40 80 120
Time (sec)
ave. 0.192
0.01−0.04 Hz
GTBY 297.88 303.92
CARI/1.00 1.00 1.00/
43.2
0.241
100.0
0.397
78.4
0.102
0 40 80 120
Time (sec)
ave. 0.247
Misfit average 0.356
2010/ 3/ 1 10:37:37.0
(18.4400, −72.7500)
Depth= 5 km Mw = 4.29
3.3971×10^22 dyne−cm
Strike Dip Slip
Plane 1: 103.97 27.50 81.93
Plane 2: 293.05 62.80 94.18
CLVD= 9.0%
N
P
GRTK
SDDR
W
E
T
B
S
Misfit
0.6
0.4
5 10 15 20 25
Depth (km)
0.0007 mm

Figure 4m

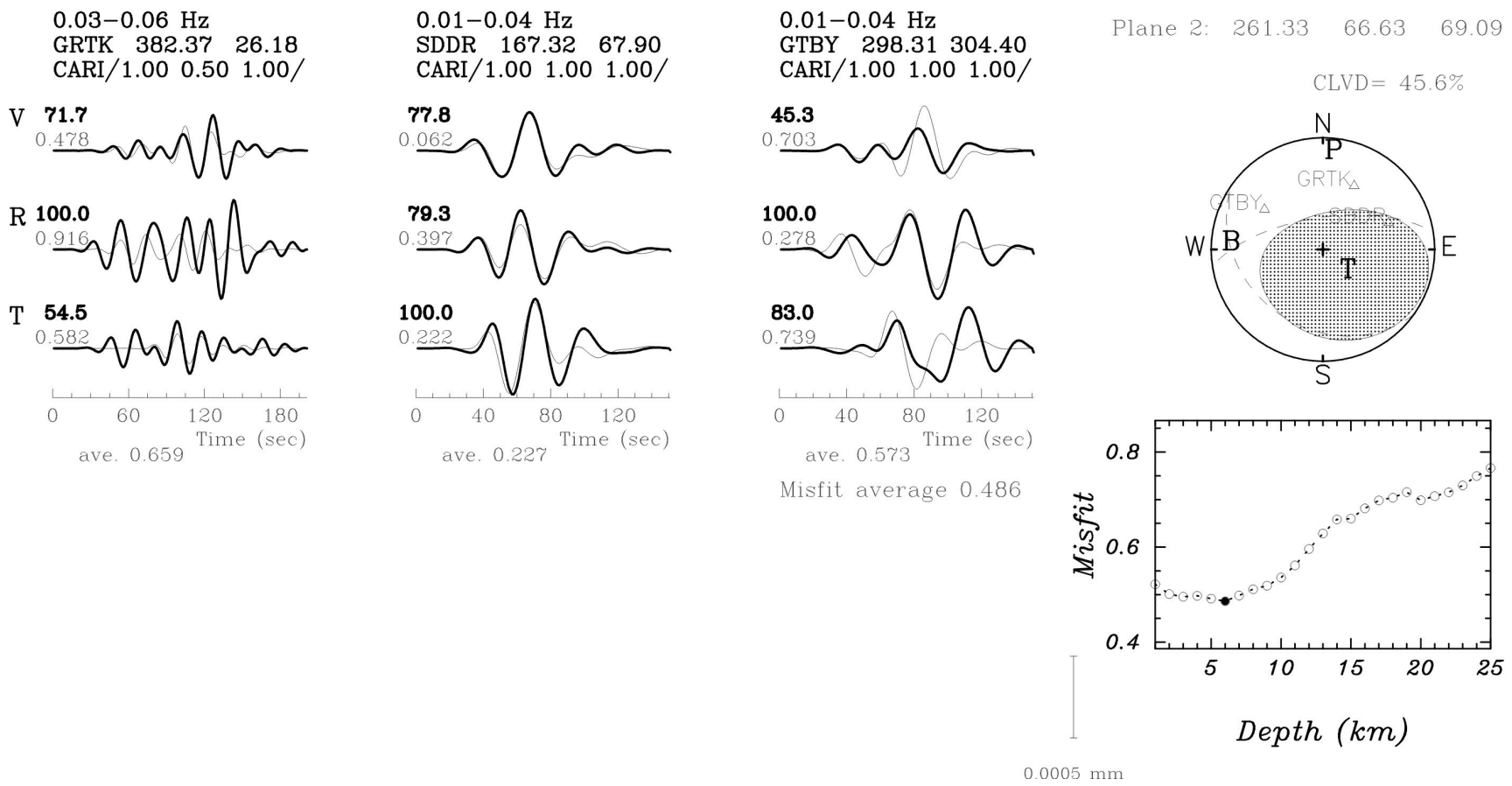
0.03−0.06 Hz
GRTK 382.37 26.18
CARI/1.00 0.50 1.00/
V 71.7
0.478
R 100.0
0.916
T 54.5
0.582
0 60 120 180
Time (sec)
ave. 0.659
0.01−0.04 Hz
SDDR 167.32 67.90
CARI/1.00 1.00 1.00/
77.8
0.062
79.3
0.397
100.0
0.222
0 40 80 120
Time (sec)
ave. 0.227
0.01−0.04 Hz
GTBY 298.31 304.40
CARI/1.00 1.00 1.00/
45.3
0.703
100.0
0.278
83.0
0.739
0 40 80 120
Time (sec)
ave. 0.573
Misfit average 0.486
2010/ 5/20 6:34:12.0
(18.4190, −72.7600)
Depth= 6 km Mw = 4.19
2.366×10^22 dyne−cm
Strike Dip Slip
Plane 1: 125.26 30.96 129.56
Plane 2: 261.33 66.63 69.09
CLVD= 45.6%
N
P
GRTK△
GTBY△
SDDR△
W
B
T
E
S
Misfit
0.8
0.6
0.4
5 10 15 20 25
Depth (km)
0.0005 mm

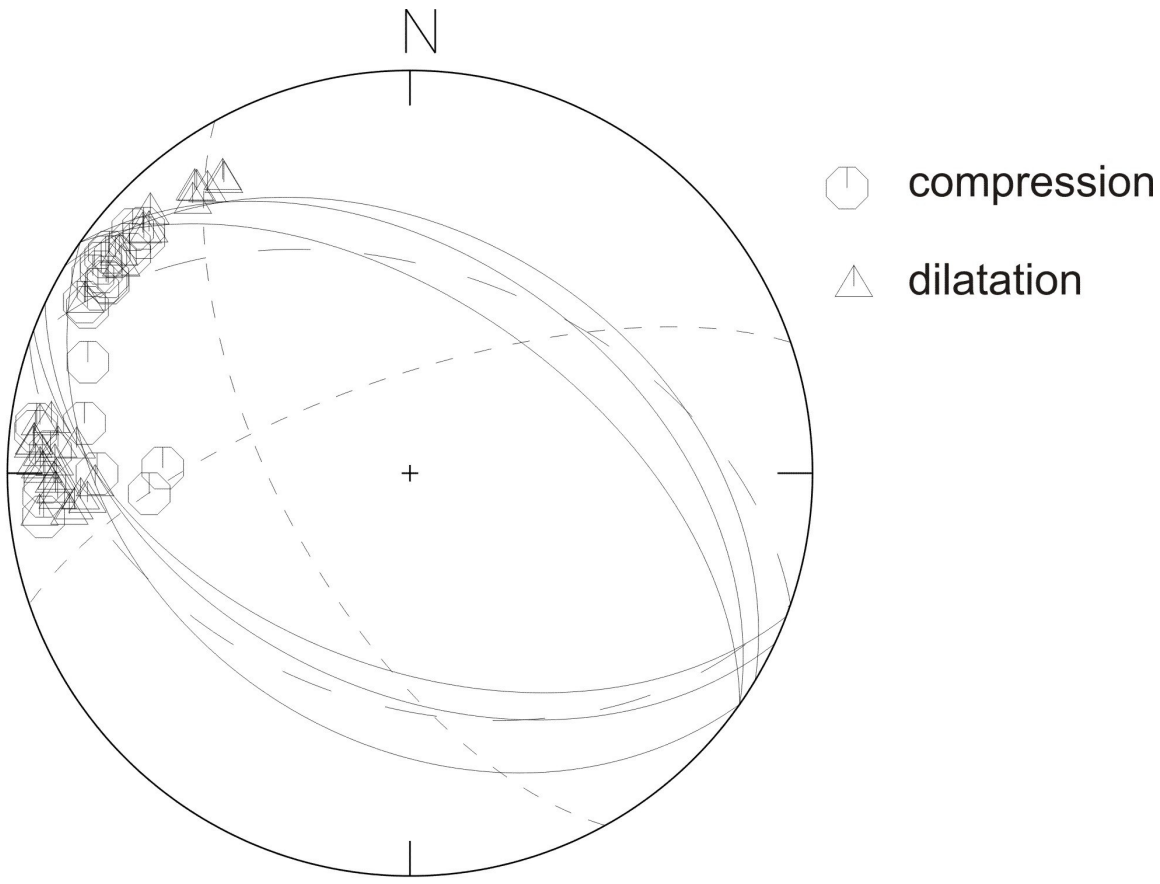

Composite Aftershock Mechanism: Western Group

Figure 5a. Composite focal mechanism from first motions of aftershocks located in the western region of the aftershock zone (see Figure 3). In this and Figures 5b and 5c the solid lines represent the focal mechanisms for the data shown, the dotted line is the Global CMT (2010) solution for the mainshock and the dashed line is the their solution for the largest aftershock.

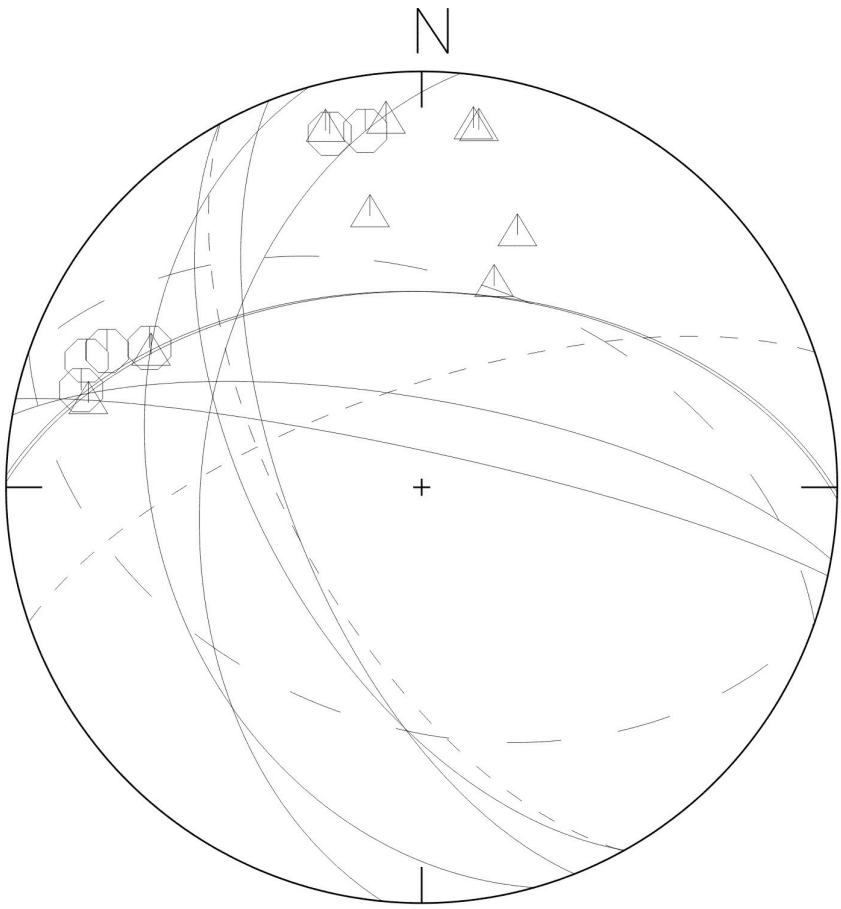

Composite Aftershock Mechanism: Central Group

Figure 5b: Composite first motion solution for aftershocks in the central region of the aftershock zone. Format as for Figure 5a.

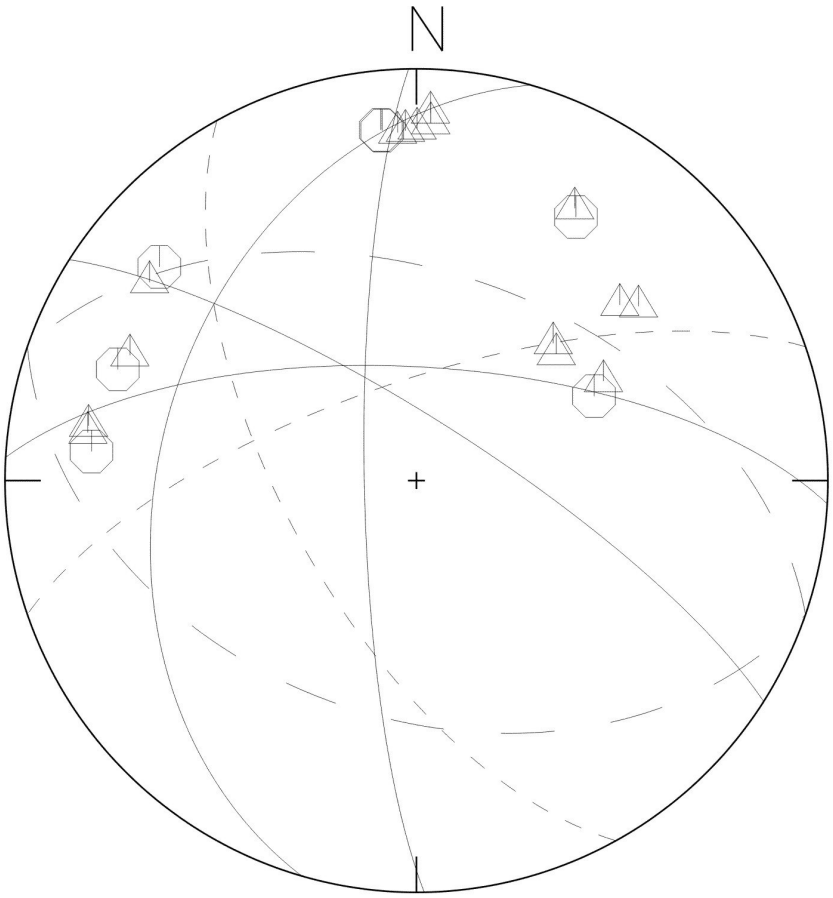

Composite Aftershock Mechanism: Eastern Group

Figure 5c. Composite first motion solution for aftershocks in the eastern region of the aftershock zone. Format as for Figure 5a.

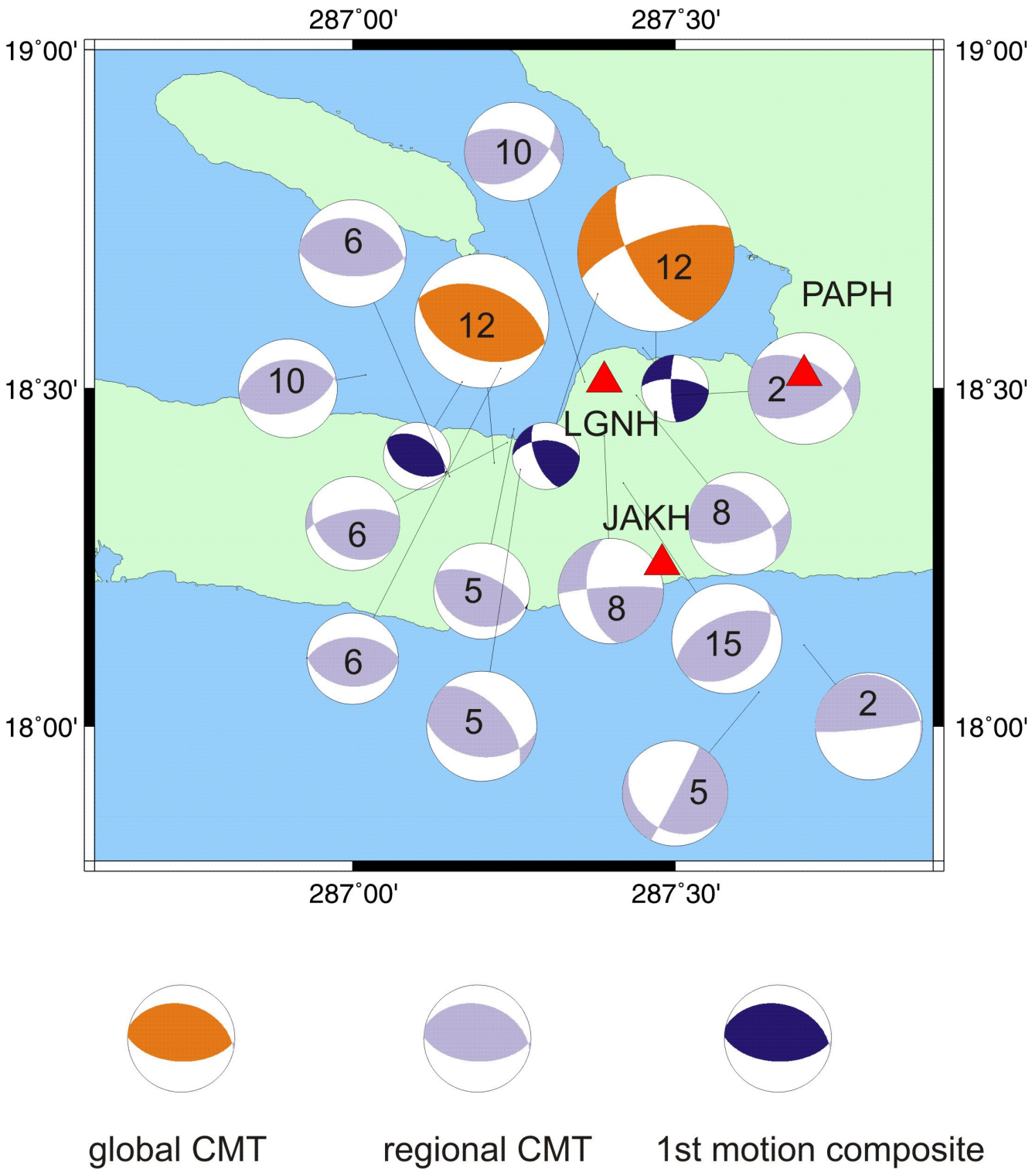

Figure 6: Summary of focal mechanisms. Symbols are scaled to moment magnitude with the composite solutions fixed at M_w 3.0. The number written on the focal mechanism solution is the modeled depth in km. Most of the events used in the composite mechanisms had depths fixed at 10 km. The focal mechanisms for the mainshock and largest aftershock (shown in orange) were determined by the Global CMT Project (2010).